AD NUMBER

AD482047

LIMITATION CHANGES

TO:

Approved for public release; distribution is unlimited. Document partially illegible.

FROM:

**Distribution authorized to U.S. Gov't. agencies and their contractors;
Administrative/Operational Use; APR 1965. Other requests shall be referred to Air Force Technical Applications Center, Washigton, DC. Document partially illegible. This document contains export-controlled technical data.**

AUTHORITY

usaf ltr, 25 jan 1972

DETECTION, ANALYSIS AND INTERPRETATION OF THE TELESEISMIC SIGNAL FROM THE SALMON EVENT

2 April 1965

Prepared For

AIR FORCE TECHNICAL APPLICATIONS CENTER
WASHINGTON, D. C.

By

Charles B. Archambeau and Edward A. Flinn
SEISMIC DATA LABORATORY

Under

Project VELA UNIFORM

Sponsored By

ADVANCED RESEARCH PROJECTS AGENCY
Nuclear Test Detection Office
ARPA Order No. 624

Export Liaison Hqs AF Wash D.C.
per telecon Col Ridenour's office 19 May 66 jwde

(6) DETECTION, ANALYSIS AND INTERPRETATION
OF THE TELESEISMIC SIGNAL FROM
THE SALMON EVENT,

(11) 2 Apr [redacted] 65,
(12) 59p.

(14) SEISMIC DATA LAB [redacted] -120

AFTAC Project No.:	VELA T/2037
Project Title:	Seismic Data Laboratory
ARPA Order No.:	624
[redacted] No.:	5810

(16) AFTAC-VELA-T/2037

[redacted]	UED EARTH SCIENCES DIVISION TELEDYNE, INC.
Contract No.:	(15) AF/33(657)-12447, ARPA Order-624
Date of Contract:	17 August 1963
Amount of Contract:	$5,257,624
Contract Expiration Date:	17 February 1966
Project Manager:	Robert Van Nostrand (703) 836-7644

(10) Charles B. Archambeau
Edward A. Flinn.

P. O. Box 334, Alexandria, Virginia

355 575

ref

This research was supported by the Advanced Research Projects Agency, Nuclear Test Detection Office, and was monitored by the Air Force Technical Applications Center under Contract AF 33(657)-12447.

TABLE OF CONTENTS

ABSTRACT

A rectilinear motion detection (REMODE) technique is used to isolate arrivals from the SALMON event at teleseismic distances in several cases where the signal-to-noise ratio is low and visual methods or the ordinary array processing procedures fail. The essential aspects of array and single station REMODE processors currently in use are described and examples from the SALMON event are shown. The phase isolation capability of the processor seems ~~most~~ promising and is fully exploited in the analysis of the SALMON data. ~~In particular,~~ P-wave travel time data are obtained from the processed traces along three azimuths from the SALMON site. The travel time curves obtained show reasonably well-defined multiple branches. An inversion method giving the velocity structure appropriate to these data is ~~briefly~~ described, and the structures obtained from the SALMON data are discussed. Radiation patterns appropriate to the primary travel time branch for the P-wave are obtained for various frequencies, and these are interpreted in terms of an ideally symmetric and purely compressional source. Comparisons are also made to theoretically derived radiation patterns for explosive sources with associated tectonic energy release.

The surface wave dispersion along the three profiles from the SALMON site has been measured and an inversion method for this data is discussed. Velocity structures appropriate to the surface wave data are described and compared to the body wave structures. Rayleigh wave radiation patterns are also obtained and interpreted in terms of a compressional source.

1. INTRODUCTION

The study to be described is primarily an attempt to incorporate travel time and amplitude measurements of first and later arrival P-waves with relatively long period surface wave observations. Such measurements are then used to obtain basic source and path information for this particular event. The study is, however, useful in a wider sense since it will be apparent that the methods and computational programs to be described are applicable to general seismological studies.

2. SCOPE AND OBJECTIVES OF THE STUDY

Some specific objectives of the analysis are the following:

(a) To measure the dispersive and amplitude characteristics of the surface waves generated by this source and the travel times and associated amplitude characteristics of first and later arrival P-waves from the source; these measurements being made primarily along selected azimuths corresponding to separate structural regions. In the present study only LRSM stations were used and Figure 1 shows the stations receiving short and long period signals from the event, along with the appropriate profiles and structural regions.

(b) To determine the appropriate variation of elastic parameters with depth. That is, the earth structure corresponding most closely to both the body and surface wave measurements.

(c) To determine source radiation patterns for seismic surface waves and for first arrival P-waves.

(d) Coupled with the structural information, to infer the affects of regional variations in crustal and upper mantle structure on the radiation patterns and amplitudes of the motion.

(e) To determine some of the source characteristics from the seismic radiation field, in particular, from measurements of mode excitation of Rayleigh and Love surface waves and from the radiation patterns of surface and P-waves.

3. PRELIMINARY OBSERVATIONS AND DATA

A few general observations concerning the source and the associated seismic field can be made from a preliminary analysis of the signal from this event.

(1) Fundamental mode Rayleigh waves were identified at 21 LRSM stations, in the period range 8 to 40 sec., out to about 2500 Km. Higher mode Rayleigh waves were observed to distances of 3000 Km on the continent and at nearly every operative LRSM station. P phases were detected at all but one or two continetal LRSM stations and at La Paz, Bolivia, at a distance of 5704 Km. The long period Rayleigh wave excitation was not very great, as might be expected, and the signal-to-noise ratio was generally quite low, except at the closest pair of stations. In addition, the occurrence of an earthquake in Mexico either complicated or completely obliterated the Rayleigh

waves at some of the western stations. Consequently, the analysis of surface wave radiation was limited to the 14 stations indicated in Figure 1. On the other hand, the quality of the short period data was uniformly good and uncomplicated by other events, so that all LRSM stations (40) were used in the body wave analysis.

(2) As with the GNOME event, no Love wave radiation was observed. This is in contrast to most of the NTS shots, for example, SHOAL and BILBY, which produce SH surface waves of this type. One may note that the presence of Love waves would be expected if tectonic energy release occurred. While NTS is in a tectonically active area, and the medium would normally be prestressed, SALMON and GNOME were in salt and would not support even a modest prestress field. Thus, the lack of SH radiation from SALMON and GNOME would be consistent with the presence of such radiation from NTS events if tectonic release were involved. The observations are still, however, open to other interpretations.

(3) P-wave arrivals along the NW profile were approximately the same as the J-B times, while on the N profile they were 4 to 5 seconds earlier, and on the NE profile, 2 to 4 seconds earlier than the J-B times. These observations were in general agreement with those from GNOME.

4. DETECTION AND ANALYSIS OF BODY WAVE P-PHASES

The analysis of the short period data was actually accomplished in several stages. As was previously indicated, the initial P and whatever later P-phases that could be detected and isolated were analyzed. Thus, the arrival times for all P-phases were computed and then Fourier spectra of first arrival phases was obtained on the basis of these times.

For detection and isolation purposes, a special filter was used to process the time series. The filter process is termed "rectilinear motion detection" and abbreviated to REMODE. The basic concepts involved in the design of such a filter are not new and several have been successfully used before, most recently on Shimshoni and Smith (1964). In addition, Mims and Sax (1965) have described several of these filters, reviewed their history, and investigated some aspects of the theory.

In simplified terms, these filters are designed so as to pass motion that is rectilinear, and to filter out elliptical motion. Thus, the motion that is in phase in the radial and vertical directions over a time equal to about one-cycle of the expected signal is amplified, while the motion that is 90° out of phase during this time is attenuated. The basis of such a filter is, of course, the assumption that the noise is predominantly made up of Rayleigh waves and that the primary P-motion, or initial part of a "P coda", is rectilinear. Furthermore, it is assumed that the remainder, or tail of the "coda" is superposed P, SV, and Rayleigh motion. In actual fact, these assumptions appear to be valid, at least to a degree, at most of the sites tested. In addition, they are

in good agreement with the independent physical evidence available to us.

In practice, the filter operates to amplify motion that is only near to being rectilinear, inasmuch as no motion is observed to be precisely rectilinear. It therefore uses the ellipticity of the particle orbit in the RZ plane, defined over a time of about one period of the expected signal, as a gain factor. In Figure 2, a schematic diagram showing an array processor indicates the way in which this filter is combined with velocity filtering (time shifting and summation) and ordinary frequency filtering. The frequency filtering is actually optional and was not used in the present preliminary application even though it is usually of considerable value. The REMODE process indicated is a relatively primitive one, but was nevertheless reasonably effective. As is indicated, the output of the REMODE filter may be fed back into the filter after a pass and the number of REMODE passes is optional. If frequency filtering is used the individual filtered traces may be displayed separately and also summed.

Analytically the REMODE filter function used may be described in terms of the even part of the cross correlation between the radial and vertical components of motion. Such a function, when used as a filter, will selectively attenuate motion on the two traces which is out of phase and will pass that which is in phase. The actual correlation function used is computed over a short time window of width 2T centered at a reference time t_o. This correlation function is then used as the filter appropriate to the time t_o. The filter is changed by recomputation of the correlation function as t_o increases,

so that the filter varies with the time t_o.

Specifically, the correlation function used is

$$\Phi_{RZ}(\tau, t_o, T) = \int_{-T}^{T} R(t') \, Z(t' + \tau) \, dt' \qquad (1)$$

with $t' = t - t_o$

The even part of the cross correlation is then computed from

$$E\{\Phi_{RZ}(\tau, t_o, T)\} = \frac{1}{2}\left[\Phi_{RZ}(\tau, t_o, T) + \Phi_{RZ}(-\tau, t_o, T)\right] \qquad (2)$$

The filter over the interval 2T can then be defined as an appropriate average, or even some function of (2); the relationship used is to some degree arbitrary. If a weighted average is used, as was the case in the present application, one has, for example,

$$C(t_o - T + \tau) = \frac{1}{2T-\tau}\left(\frac{1}{2}\left[\Phi_{RZ}(\tau, t_o, T) + \Phi_{RZ}(-\tau, t_o, T)\right]\right) \qquad (3)$$

This filter is then convolved with the original Z and R component time series in the interval 2T in the normal manner, except that only the first point in the filtered time series is retained. Thus, in the present application, the REMODE Z component at the time $t_o - T$ (the beginning of the interval about t_o) is taken to be

$$Z^{(1)}(t_o - T) = \int_{0}^{2T} C(t_o - T + \tau) \, Z(\tau) \, d\tau \qquad (4)$$

This gives one point of the filtered series and the next is obtained by allowing (τ_o) to increase (incrementing t_o by a finite amount in the digital case) and proceeding through the computations indicated by (1) through (4) once again.

This general type of filter may be termed a time varying linear filter. In the present application the immediate future of the particle motion is used to design the filter. It is clear that the criteria of recilinearity may be incorporated in a filtering process in a variety of ways. The procedure described in this study is only one of many possible methods. It was however, the first that has been applied to a relatively large amount of data. More recently several other REMODE processors have been designed with somewhat greater phase isolation and selectivity capabilities, and their application to time series data is now in progress.

Figure 3 shows two especially good examples of the signal-to-noise enhancement and phase isolation capability of the filter. The traces shown correspond to single LRSM stations, so that the array processor indicated in Figure 2 degenerates to a simple double application of the REMODE filter in this case. The event shown is SALMON, and the stations are in the 20° distance range and, as might be expected, several clear P arrivals have been isolated, presumably corresponding to an inverse branch or multiple branches of the travel time curve. As was previously pointed out, these filtered traces should correspond, for a properly designed REMODE filter, to the nearly rectilinear first motions of the individual phases.

Of the stations processed in this study, roughly 30 percent gave REMODE outputs with S/N enhancement and phase isolation

comparable to the examples shown.

The most common failing in the remaining processed records, aside from occasional reductions in the overall signal to noise enhancement feature of the process, was the absence of a clearly isolated P_n arrival in the zone where the S/N ratio for P_n is low. While this apparent lack of sensitivity may be due to the manner of data presentation (i.e. the scaling of the plotted filter output), it most likely indicates a threshold of S/N for detectibility, with this particular filter at least. The precise threshold limits are observed to vary from location to location however, so that one must conclude that the character of the noise and signal, but especially of the noise, determines to a great extent the sensitivity of the filter to small amplitude rectilinear signals.

Figure 4 provides some indication of the detection sensitivity of the process under what are probably ideal noise conditions. The records shown are from the Oslo, Norway array at a distance of 7565 kilometers from SALMON, well beyond the range of detection by simple visual or analytical correlation methods. Approximately four minutes of record were used from each trace two minutes before and after the predicted P arrival time. Only a section of this time interval is shown in the Figure. Before application of the REMODE filter none of the array detectors show the signal, nor does the velocity filtered trace.

Two passes through the REMODE filter provides optimum noise reduction and in this case gives two arrivals at approximately the times predicted for P and PcP. No other pulse

besides these two, or in fact motion of any sort, was observed on the 2nd pass REMODE trace during the 4 minute time sample. It seems reasonable to conclude that these pulses result from the arrival of signals from SALMON.

The actual shape of the pulse passed by the filter is likely to be quite distorted, especially when the S/N ratio is low, since, in addition to distortions introduced by the filter itself, the sum of the noise and signal is admitted, inasmuch as the filter acts somewhat like a gate. Hence, this filter provides information on the time of first motion and the interval of rectilinearity for a phase but little highly reliable information on the pulse shape. Indeed one might expect the signal as admitted by a REMODE filter to look much like a section of the noise when the S/N ratio is low. This appears to be the case with the REMODE trace for the Oslo array, although the true shape of the pulse is itself unknown.

5. INTERPRETATION OF P-WAVE AMPLITUDE SPECTRA AND TRAVEL TIMES

The arrival times and time intervals of rectilinear motion for the phases as indicated by the REMODE processed time series were correlated with the original unfiltered records in order to verify the body phases obtained. The travel times of the phases were then plotted as functions of distance along the three profiles indicated on Figure 1. In addition, the interval times were used to "velocity window" the original time series and so provide samples of the rectilinear part of the individual arrivals. Fourier spectrums of the observed first arrivals at all profile stations were then computed.

Figures 5 through 8 show P-wave spectra at several distances along the N. W. profile. The spectra have been corrected for instrument response and should provide an accurate estimate of the direct P-wave ground displacement with minimal contamination from reverberation effects. The change in spectral content of the examples shown is due, in part, to differences in wave type, that is, P_n compared to P, as well as from distance affects on the amplitude. In particular, Figure 5 shows P_n spectra at a distance range where P_n is yet the first arrival, whereas Figure 6 through 8 correspond to direct P-arrivals. It is clear that the maximum spectral amplitude for P shifts to longer periods with increasing distance, due to the roughly linear increase in attenuation with frequency. The observed attenuation will, of course, be affected by the variation of the dissipation function Q with depth in the earth (e.g. Anderson and Archambeau, 1964) so that the attenuation will be dependent on the actual minimum time path followed by the phase. This effect would be of second order, however, compared to the much larger amplitude affects associated with the velocity variations with depth, particularly with velocity reversals and rapid or discontinuous charges in velocity.

Thus, the observed spectra would not be expected to fall off uniformly with distance in the range where the minimum time paths would be strongly affected by the velocity variations in the upper mantle of the earth. Indeed, strong and rapid variations with distance would be expected in view of the likelihood of large gradients in the velocity variation with depth and the existence of the low velocity zone in the upper mantle.

A comparison of spectral amplitude with distance at particular frequencies is given in Figure 9. The anomalous behavior only suggested by the previous individual spectra is now quite apparent. The essential aspects of the amplitude-distance variation obtained and illustrated in this figure have been observed many times before by other investigators, and in particular, for events observed along a profile of stations in this same region (e.g. Romney et al., 1962). The spectral detail in the present case is perhaps somewhat greater than has been available before, so that a correspondingly more detailed interpretation will be advanced.

The spectra will be interpreted together with the observed travel time curves. However, viewed independently, they show a fairly rapid fall-off with distance out to approximately 1250 kilometers. The rather gradual increase in amplitude, beginning at this point and reaching an apparent maximum at 1800 to 1900 kilometers, probably indicates a first arrival P-phase different from P_n. A decrease in amplitude at around 2000 km, followed by a second peak in the spectrum again probably indicates a second P-phase.

This rather superficial interpretation will be checked with the travel time observations for evidence of changes in the first arrival curve slope as well as for the existence of multiplicities or cusps in the curves accounting for the amplitude maxima.

Figure 10 shows the travel-time versus distance data for the N. W. profile; Figure 11 the time distance data for the combined North and N. E. profiles. Figure 12 shows the data for all profiles combined. The data shown correspond to

first arrival phases and all phases within 20 seconds of the first arrival at a given distance, with the exception of those identified as PP and PPP. At the greater distances some of the later arrivals are shown since they were often of large amplitude and may be related to mantle velocity variations which manifest themselves in the first arrival curve at somewhat greater distances than those considered in the present study. Figures 13 and 14 show the travel time observations obtained for PP and PPP from the REMODE processed time series. They have the expected character as functions of distance and serve, in part, to increase the confidence with which one may interpret the travel times for other phases, particularly the P_n and P travel times.

The solid circles in the figures indicate large amplitudes arriving at a particular distance, open circles relatively small or moderate amplitudes. The other symbols refer to J-B travel times.

The travel time curves drawn through the data are based on the travel time data themselves and the previously discussed amplitude-distance spectra. In addition, the curves correspond in their general characteristics to theoretical curves obtained from the velocity structure shown in Figure 15. The initial selection of this structure was based upon a consideration of the long period surface wave dispersion data obtained by a number of investigators and compiled by Anderson and Toksöz (1963). The velocity structure in the mantle is a modified version of the CIT 11 oceanic model proposed by Anderson and Toksoz to explain the Love wave dispersion data. The model has also been found to provide good amplitude and travel time agreement with independent body wave data (Anderson, personal communication).

The only extensive modification to their structure is the addition of a crustal section - and of course, conversion to compressional velocities, which involves assumptions of Poisson's ratios. Thus, in view of the essential agreement between continental and oceanic dispersion for periods beyond about 50 seconds, the model agrees with continental long period surface wave dispersion.

While the structure has been checked and perturbed somewhat for consistency with the P phases observed, no particular effort has been made to adjust the fit to the P_n and other body phase data except in an approximate manner. For this reason, the structure shown should be regarded as a preliminary fit, which must be adjusted to account more fully for P_n, the reflected P phases, and the finer details of the direct P phases. In addition, the crustal section used here corresponds to an average crust which, for a finer fit, would have to be replaced by the crustal section appropriate to the particular region or regions involved in the travel time profile. Initial crustal and upper mantle models would come from the inversion of the shorter period (10 to 50 seconds) surface wave dispersion data considered in a later section of this report.

Nevertheless, a fairly consistent explanation of all observations emerges from a comparison of the travel time data with the amplitude-distance spectra and the surface wave structure. In particular, the Northwest profile travel times indicate a retrograde branch beginning at about 1500 km. and extending back to a cusp near 750 km. at which point a forward branch of the curve begins (P_1) and eventually intersects the P_n curve. This

multiplicity in the P curve is due to the low velocity zone indicated in Figure 15, the location of the cusp being controlled primarily, in this case, by the steep velocity increase beginning at about 130 km. Theoretically one would expect large amplitudes in the neighborhood of the cusp, diminishing rather rapidly with increasing distance along the travel time curve on the forward branch. This in fact is indicated by the relative amplitudes observed and shown on the travel time curves. The intersection of the P_n and P_1 curves at approximately 1300 km seems well defined by the double arrivals corresponding to P_n and P_1 at the GV, FO, RT and LC stations. In addition the amplitude-distance spectra show a marked increase in amplitude of the first arrivals, beginning at 1300 km.

At distances smaller than 1300 km, P_n is the first arrival and the amplitude-distance spectra indicate a rapid fall-off with distance for the P_n energy at .7 cps. On the other hand, the energy at higher frequencies, although lower in amplitude, shows no such large slope. This would seem to delimit thickness of the upper mantle high velocity "lid" between the low velocity zone and the Moho, since the longer period energy could be considered to leak into the low velocity zone, while that at shorter periods would not be nearly so much affected. However, the amplitude-distance spectral data in the epicentral range in question does not provide a dense enough distance coverage to enable us to draw very definite conclusions. The extension of P_n to 1300 km., and beyond that to at least 1600 km as a second arrival, must imply a fairly thick lid on the low velocity zone, as was pointed out by

Lehmann (1964), otherwise P_n would attenuate far too rapidly with distance to be observed even by a sensitive filter technique. In the extreme case, P_n could not exist at all. In view of the present data this mantle high velocity section need not be extremely thick, of the order of 15 km (Lehmann 1964), but is probably thicker than that indicated by the structure of Figure 15.

Beyond 1300 km., P_1 is the first arrival and is definitely observed out to about 1600 km. on the N. W. profile, with P_n as a second arrival. At greater distances P_1 arrivals are not detected on this profile, and the branch indicated as P_2 are the apparent first arrivals. However, the P_2 arrivals in the region of the cusp at 1700 km. have very large amplitudes while P_1 should be relatively small. It is quite possible that the P_1 signals were weak enough compared to the noise and near enough in time to the large P_2 arrivals so as to be undetected either by visual or REMODE processing. Hence the presence of P_1 beyond 1600 km. can only be inferred on this profile. On the N. profile in Figure 11 however, an arrival at station GP, at 1865 km., corresponds to P_1. The consistency of this arrival with all other P_1 arrivals is shown in Figure 12 where the data from all profiles is combined. Although at least one other interpretation is possible, it appears that reasonably good evidence exists for the presence of this P_1 branch and its extension out to approximately 2200 km. as a first arrival. In addition, while the P_1 amplitudes would be large near the cusp due to the low velocity zone, the amplitudes would be expected to fall off quite rapidly with distance.

The second multiplicity in the P travel time curve, having P_2 as its forward branch, is due to a rapid increase in the velocity gradient and can be accounted for in terms of the marked velocity increase near a depth of 330 km. in Figure 15. The observed travel times suggest that the multiplicity is a triplication, the P_1 branch joining the retrograde P_2 branch to form a cusp. The forward cusp has very large amplitudes associated with it and is undoubtedly a caustic. While the only direct evidence is the relative amplitude estimates for the arrivals at the relevant stations, it appears that the more distant cusp is also a caustic. This implies that the variation of the velocity gradient and the velocity itself are both continuous, since otherwise both cusps could not be caustics. Such a conclusion, however, is only tenative in view of the need for many more observations of both travel time and amplitude, and the lack of detailed spectral estimates for the later arrivals near the more distant cusp. If the second cusp is not a caustic, then the velocity gradient changes discontinuously at around 330 km. rather than continuously. On the other hand, if neither cusp were a caustic, a discontinuous jump in velocity would be implied (Bullen, 1961). In view of the amplitude-distance spectral peak in the zone near the forward cusp, this latter velocity structure seems unlikely.

The details of the amplitude-distance spectra in Figure 9 can be interpreted in a manner quite consistent with the previous travel time interpretation. Thus the spectral increase in amplitude at 1300 km. is due to the emergence of

the P_1 branch as the first arrival, but the continued rise to the point at 1800 km. is associated with P_2. Therefore, the implied maximum in P_1 is only apparent since P_2 was picked as the first arrival instead of P_1. The actual first arrival, P_1, undoubtedly has a low amplitude at this distance and would in any event have its largest amplitude where first measured at around 1300 km. The shift toward shorter distanced of the spectral maximum associated with the P_2 branch's cusp on the higher frequency curve (1.3 cps) again indicates the frequency dependence of absorption in the earth. That is, the attenuation of the higher frequencies with distance of propagation is large enough to cause the maximum in this first arrival amplitude curve to appear to rise very sharply and then to decrease rapidly with distance. Actually, of course, the amplitude-distance curve plotted only for P_2 would have its maximum at the cusp near 1700 km. The spectrum of Figure 9 then shows that the higher frequencies fall off with distance away from the cusp at a much greater rate than do the lower frequencies; this effect is due to absorption. The net effect, when only first arrivals are used, is to produce a jump in the amplitude curve at the transition from P_1 to P_2. For high frequencies, the amplitude versus distance curve for first arrivals should then fall off rapidly, producing a clear maximum at the transition, while for lower frequencies the maximum should appear at the transition, but it should be much less conspicuous (i.e. broader), since the attenuation with distance is much smaller. Figure 9 shows this effect, the transition occurring at about 2200 km.

Both the spectra shown in Figure 9 show a minimum at 2000 km. which cannot be readily explained on the basis of the present interpretation of the data. There is the possibility that P_1 is late at the station involved, and has been used for the spectral estimate, although it would have to be as much as 3 seconds late. Alternately, the observed minimum could be station effect, an instrumental effect, or it could be due to interference between nearly simultaneous arrivals. The question cannot be resolved without more data.

The possibility that P_1 is late at distances beyond about 1700 km. on the Northwest profile and that a cross-over from P_1 to P_2 occurs at around 2000 km. does however suggest that P_1 is present and was detected beyond 1600 km. but that the whole P_1 curve was shifted by about 3 seconds to later times. The delay could then be attributed to a crustal thickening under the Rocky Mountains and a simultaneous deepening and extension of the low velocity zone. Again, more data is necessary in order to test such a hypothesis.

Such considerations naturally bring us to a comparison of the observations between the profiles. Since the North profile coverage was so sparce, it was combined with the Northeast profile. Even so, the total number of stations used was small, so that conclusions concerning structure and the very nature of the travel time curves are much more tenative than for the previous profile.

In general, the North-Northeast profile appears to be similar to the Northwest profile. There seem to be, however, a number of differences which can be summarized as follows:

(a) The P_n velocity is slightly higher on the North-Northeast profile than on the Northwest profile.

(b) The duplication in the travel time curve associated with the low velocity zone is not so well defined, and appears to be less pronounced. This would imply a smaller velocity decrease and a shallower bottom to the low velocity zone. A similar conclusion is also suggested by the surface wave dispersion data obtained.

(c) Observations of P_1 out to 1900 km., and again on either side of the transition to P_2 at 2165 km., indicate that P_1 can be detected over its entire range of existence. It also suggests either that the amplitudes of P_1 along the N. W. profile were relatively small or else that the P_1 times were in fact all delayed beyond about 1600 km. from the source. In either case, structural differences beginning at the bottom of the low velocity zone are implied.

(d) The triplication in the travel time curve is quite well defined and does not differ significantly from that observed from the N. W. profile.

Average travel time curves for all profiles are given in Figure 12. The figure also serves to indicate the consistency of the phases isolated by the special filter utilized in this study.

Comparison of the travel times with the Jeffreys-Bullen travel times for all profiles and stations shows that the J-B times are averages between the two arrivals on the P duplication due to

the low velocity zone. They are consequently late compared to P_1. They also represent averages for the two branches of P_2 on the triplication. Thus, P_1 appears to be ignored, and when present with sufficient amplitude or when not too close in time to the P_2 arrivals as is the case on the North and Northeast profiles, then P_1 will provide early first arrival observations. This of course is the case on the North and Northeast profiles; in the west, P_1 is late, has small amplitude, or both, so that the J-B times tend to agree quite closely with the observed first arrival times. In all cases the J-B times agree closely with the travel time curves given here in regions where they are single valued.

6. INVERSION OF BODY WAVE DATA BY PERTURBATION METHODS

In view of the emphasis placed on the structural interpretation of the travel times in the preceding discussion, it seems relevant to indicate briefly the manner in which one can deduce velocity structure from the travel time data.

The classical methods of course are available, but are especially cumbersome if not impossible when later arrivals, corresponding to multiplicities in the travel times, are to be used. Many investigators have therefore adopted trial-and-error perturbation methods utilizing the inherent speed of a digital computer to arrival at a suitable approximate fit. The situation is similar to that experienced by those searching for structures in agreement with the observed surface wave dispersion. In this later case, numerous authors have proposed perturbation methods for fitting the surface wave data (e.g. Anderson, 1963, Archambeau and Anderson, 1963). As might be expected, a similar procedure may be applied to the body wave travel times. The procedure here differs from

that proposed by Bullen (1960) in not involving a layer approximation to the velocity distribution.

In particular, we assume that an initial structure has been chosen which gives travel time curves resembling those observed. The velocity variation with respect to the earth's radius is then fitted by a function or a set of sectional functions of the form

$$V(r) = \sum_j \alpha_j \left[F(r) \right]^j \qquad (5)$$

with V denoting the appropriate velocity. It is then easy to prove the following relation involving the travel time T, the perturbations of residuals in the travel times δT, the coefficients, α_j in (5) and their variations $\delta\alpha_j$ (Archambeau and Flinn, 1965)

$$\left(\frac{\delta T}{T}\right)_\Delta = -\sum_j \left(\frac{T_j}{T}\right)_\Delta \left(\frac{\delta \alpha_j}{\alpha_j}\right)_\Delta \qquad (6)$$

with

$$T_j = -\alpha_j \left(\frac{\delta T}{\delta \alpha_j}\right) = 2 \int_{r_p}^{R} \left(\frac{\alpha_j \left[F(r)\right]^j}{V(r)}\right) \frac{r\, dr}{v^2 \left\{\frac{r^2}{v^2} - \frac{r_p^2}{v_p^2}\right\}^{1/2}} \qquad (7)$$

and where

$$T = \sum_j T_j \qquad (8)$$

The subscript Δ is used to imply an evaluation at fixed distance Δ. The integrand in (7) corresponds to the usual form for the computation of the travel time for a ray in an inhomogeneous

sphere of radius R, with the exception of the weighting factor $\alpha_j \left[f(r) \right]^j / V(r)$.

Thus, T_j corresponds to a contribution to the travel time due to the term $\alpha_j \left[f(r) \right]^j$. The equation (8) shows this as well.

The procedure is thus to measure the residuals between the initial starting structure and the data and to invert the system of equations of the type (6). In this manner one obtains the required corrections $\delta\alpha_j$ to the initial structure.

7. INFERENCES OF SOURCE PROPERTIES FROM BODY WAVE RADIATION PATTERNS

The amplitude spectra discussed in section (5) may also be used to provide estimates of the symmetry of the source radiation pattern. In view of the anomalous behavior of the P_2 arrival amplitudes they should and will be considered separately in this discussion. Likewise P_1 could be separated from P_n so that the three separate phases, with their relavent amplitudes, could be studied. Ideally, spectra of P_2 and P_1 obtained along the whole forward branch of their respective travel time curves should be obtained, along with spectra for P_n over its entire range of observation. In this way a greater distance range could be covered for each phase.

In the present preliminary study of the radiation patterns, only first arrivals are used, and the P_n and P_1 data are combined. However, it is easy to envision the separate P_1 and P_n patterns from the contour diagrams given.

Figure 16 shows the radiation pattern in the form of an amplitude contour diagram for the combined P_n and P_1 data. The contour intervals are based on a $1/R^3$ scale for convenience.

Here the P_1 arrivals are separated from the P_n arrivals on the basis of amplitude only. The division lines between P_n and P_1, P_1 and P_2 correspond to amplitude jumps and are found to agree reasonably well with the intersections of the P_n, P_1 and P_2 travel time curves. The western end of the P_1-P_2 curve is somewhat contorted and uncertain due again to uncertainties in identification of the phases.

Figure 17 shows the radiation pattern for P_2. The irregularity of the pattern is considerably greater than for either P_n or P_1. The lack of good control and the preponderance of stations close to the line of discontinuity with P_1, particularly for the Arizona stations, are probable causes of variance in the pattern. In addition, noise contamination at the extreme distances is probably large enough to affect the amplitudes estimates appreciably.

Nevertheless, taken together, the individual patterns are remarkably regular and show a strong circular symmetry about the source. There can be little doubt from this evidence that the source radiated compressional wave energy as would an idealized explosive source. This conclusion is supported by the absence of Love wave excitation and also by the observed circular symmetry of the Rayleigh wave radiation (Figure 21).

The actual departure from ideal circular symmetry of the Rayleigh wave radiation takes the form of a general shift of the pattern to the east; one observes that the travel times for P_1 and P_n are early in this zone. Thus, as other investigators have noted, early arrival times are correlated with large amplitudes. This correlation can be explained in terms of higher relative velocities and higher Q within the low velocity zone,

and a shallower bottom of the low velocity zone to the east and north of the SALMON site. This explanation is consistent with the hypothesis discussed above, concerning delay in the P_1 travel time in the Rocky Mountain region.

It might also be noted that the mildly anomalous behavior of the P_1 amplitudes near the P_n-P_1 transition suggests either rather marked structural variation, or else that the P_1 amplitude is not a maximum at the P_n-P_1 intersection and actually reaches a maximum at a somewhat greater distance. Again, more data is required for the resolution of this question.

While circular symmetry for an explosive source is to be expected in theory, departures of the compressional and surface wave radiation patterns from such symmetry can and usually do arise. Specifically, regional and local variations of structure, strong structural anisotropy or inhomogeneity in the source region, or tectonic release can contribute to strong variations in symmetry and amplitude.

Tectonic release has, for many of the past NTS explosions, been suspected of contributing anomalous shear wave radiation (Press and Archambeau, 1962; Toksoz, Ben Menahem and Harkrider, 1964). Figure 18 shows the theoretical dilatation and rotation amplitude patterns, due only to tectonic release, to be expected from an explosion of about the SALMON size, in prestressed media (Archambeau, 1964). These particular patterns arise from a pure shear prestress field and the total dilatation field is given by the superposition of the spherically symmetric dilatation due to the explosion and the quadrapole part due to tectonic release. The rotational part of the field is anomalous in that it is due, in total, to tectonic release. The total

energy in the tectonic radiation field is about equivalent to that expected from a magnitude 4.5 event. Thus noting that the dilatation amplitudes are an order of magnitude less than the largest rotational component, one expects a .0% perturbation in the explosive dilatation field. On the other hand, the Love wave radiation would be due entirely to tectonic release and the Rayleigh wave radiation would have a 50% or more variation due to tectonic release.

A small change in the compressional field, in the manner indicated by Figure 18, could probably not be detected in the P wave data from SALMON. On the other hand, the absence of Love waves and the symmetry of the Rayleigh wave pattern in Figure 21 indicates little or no tectonic release, inasmuch as large effects would be expected. In addition, both the Rayleigh wave and body wave data show the same shift in pattern to the east, strongly implying a regional structural variation as the source of the affect.

Thus, the P wave radiation pattern would not normally be expected to show the affects of tectonic release. However, in view of the surface wave evidence, it seems unlikely that tectonic release of any magnitude occurred with the SALMON event and that all perturbations in the amplitudes of the body phases are associated with regional structural variations and are not due to asymmetry in the source radiation pattern.

8. ANALYSIS OF SURFACE WAVE EXCITATION AND DISPERSION

Vertical component long-period records of Rayleigh waves from SALMON (as we have pointed out, no Love waves were observed) were analyzed with a recently completed digital computer program called SWAP-8. The analytical results will be the subject of a

later report; in this section we will merely describe the program and briefly summarize the excitation and dispersion data.

The Seismic Wave Analysis Program, version 8, evolved logically from an earlier analysis program written by Alexander (1963). The objective of Alexander's program was to separate surface wave modes from one another by splitting up the group velocity-period plane into rectangular cells. This splitting was accomplished by a combination of group velocity windowing of the records, and application of flat-topped band-pass digital filters. Within each such cell the program computed group velocity (by the usual scheme of counting zero-crossings) and Fourier amplitude and phase spectra. Alexander suggested the desirability of greater resolution in period than could be achieved with the fairly broad-band convolution filters then available. The basic difficulty devolved from an aspect of the well-known frequency-time uncertainty principle: a record short enough to provide adequate group velocity resolution in period was generally to short to allow narrow-band convolution filterings.

To overcome this difficulty, we have used high-Q recursive band-pass filters to achieve a very high precision in period using a long time sample. We determine group arrival times from the envelope maxima of the narrow-band filtered record. The preliminary results suggest that several higher modes, overlapping in time, can be resolved by this method.

The recursive filter has the same ring time, or response time, of an equivalent convolution filter. The advantage of the recursive filter is that it can meaningfully be applied to a record orders of magnitude shorter than its response time, since

in the present situation we are solely interested in the time of occurrence of the envelope maxima. The recursive filter is made phaseless (i.e., the time of envelope maximum is left undisturbed) simply by filtering the record forwards and then backwards.

In addition to the usual procedures for group velocity determination, surface wave data at distances close to the epicenter required careful correction for instrumental group delays. The program therefore makes this group delay correction and in addition corrects the signal amplitude spectrum. Further, noise spectral estimates are made and applied to the signal spectra for unbiased signal estimates.

Figures 19 and 20 are a schematic representation of the preliminary processing, spectral estimation, and group velocity determination of our program. The boxes marked "save" show quantities which are stored on BCD magnetic tape for subsequent use by other programs. We take up first the preliminary processing and spectral estimation portions of the program.

The raw record is filtered, decimated, detrended, and tapered. Post-decimation record length allowable by the size of the CDC 1604 core memory is 7000 digital samples, which is adequate for ordinary long-period LRSM records over paths of continental length.

The signal portion of the raw record is specified by a group velocity interval based on prior knowledge of the epicentral distance, event origin time, and the general type of crust and upper mantle structure traversed by waves of the period range to which the instruments respond. The Fourier amplitude and phase of the signal are computed at arbitrarily

close periods using a routine of Alexander's (1963). The seismometer system peak magnification is applied, to convert the amplitude spectrum of the signal to millimicrons of ground motion.

The instrument response parameters for the LRSM stations are known from the station logs, and the complete instrument phase and amplitude response characteristics can be computed from the seismometer free period and damping factor, electronic filter characteristics, and seismometer-galvanometer coupling factor. The total instrument response is calculated from these parameters, and the signal spectra corrected for instrument response. The instrumental group delay is given by the slope of the system phase response. For the LRSM long-period instruments, the group delay ranges from about 3 seconds to 20 seconds in the pass-band of the instruments - a significant influence on computed group velocity for distances of the order of a few hundred kilometers.

The spectrum is also computed of a segment of the raw record judged to contain only noise, the segment being selected to have roughly the same time duration as the signal segment, to lie reasonably close in time to the signal segment, and to avoid known times of body wave arrivals. The noise estimate is used in two ways: first, to correct the signal amplitude estimates; second, to limit group velocity calculations to period ranges in which the signal-to-noise ratio is large. If this latter application is omitted, the group velocity determinations are degraded by the noise.

We have found a signal-to-noise ratio of 2 to work well in practice. The program compared the signal and noise amplitudes spectra, and selects those period bands in which the signal-

to-noise ratio is higher than the pre-selected value. The core memory size of the 1604 allows up to 350 narrow-band filters to be applied to the windowed data (when higher modes are present, the construction of the program makes it desirable to limit the number of comb filters to about half this number). The Q of these filters is an input parameter; we have found a Q of 500 to work well in practice. A much lower Q does not yield sufficient period resolution; a much higher Q tends to lose group velocity resolution through a frequency-time uncertainty principle.

The center frequencies of the filters are distributed uniformly throughout the several period bands in which the signal-to-noise ratio is adequately high. For each comb filter, the times of envelope maxima are tabulated, corrected for instrumental group delay, and tabulated as group velocity arrivals. We have tried a number of different procedures for picking the envelope arrival times, including calculation of the quadrature function from the Hilbert transform of the signal segment. The procedure deemed most satisfactory in practice involves fitting a parabola to successive envelope extreme and tabulating the parabola peak times subject to certain acceptance criteria.

We are limited at the short-period end of the response range by the consideration that any scheme for picking envelope maxima breaks down if the envelope function contains frequencies approaching the carrier frequency; we have found this breakdown to occur at periods of about seven seconds on records where higher modes appear to be present.

The examples shown in Figure 20, for JE-IA, are typical of the group velocity determinations. Fluctuations occurring

at longer periods are presumably noise-induced. There is a clear suggestion of a higher mode present at shorter periods.

Interpretation of these group velocity determinations presents considerable practical difficulties. The group velocity at these short periods is notoriously dependent on details of the sedimentary crustal structure, and it should be observed that we apparently have dispersion data valid to considerably less than one percent.

On the other hand, it would seem that these group velocity observations could be made to yield very precise information on crustal and upper mantle structure, using an inversion perturbation technique. Theoretical derivation of the inversion coefficients for Rayleigh wave group velocity is therefore recommended as the only feasible practical means of making fullest use of these observations. It should be noted that where higher modes are observed, the widely installed LRSM long-period instruments, peaking at 25 seconds period, will furnish structual information down to at least the top of the low velocity zone, and probably somewhat deeper. The structural precision using an inversion scheme ought to be at least of the order of magnitude achievable using refraction shooting.

One immediately available application of the calibrated surface wave spectra is determination of the fundamental mode Rayleigh wave radiation patterns. Figure 21 shows the fundamental mode Rayleigh wave excitation for SALMON. The data are consistent with the circular symmetry predicted for an explosion, as was previously noted.

REFERENCES

1. Alexander, S. S., Surface Wave Propagation in the Western United States: Ph.D. Thesis, California Institute of Technology, Pasadena, California, 1963

2. Anderson, D. L. and Toksoz, M. N., Surface Waves on a Spherical Earth: 1. Upper Mantle Structure from Love Waves: J. Geoph. Res., vol. 68, pp. 3483-3499, 1963

3. Anderson, D. L. and Archambeau, C. B., The Anelasticity of the Earth: J. Geoph. Res., vol. 69, pp. 2071-2084, 1964

4. Anderson, D. L., Universal Dispersion Tables: Bull. Seis. Soc. Amer., vol. 54, pp. 681-726, 1964

5. Archambeau, C. B. and Anderson, D. L., Inversion of Surface Wave Dispersion Data: Pub. Bur. Central Seis. Intern., Ser. A, vol. 23, pp. 45-54, 1963

6. Archambeau, Elastodynamic Source Theory: Ph.D. Thesis, Califronia Institute of Technology, Pasadena, California, 1964

7. Bullen, K. E., Seismic Ray Theory: Geophysical Journal, vol. 4, pp. 93-105, 1961

8. Bullen, K. E., A New Method of Deriving Seismic Velocity Distribution from Travel-Time Data: Geoph. J., vol. 3, pp. 258-269, 1960

9. Flinn, E. A. and Archambeau, C. B., Inversion of Love and Rayleigh Wave Group Velocity Dispersion Data: unpublished Seismic Data Laboratory Memorandum, 1965

10. Kovach, R. L. and Anderson, D. L., Long-Period Love Waves in a Heterogeneous Spherical Earth: J. Geoph. Res., vol. 67, pp. 5243-5255, 1962

11. Lehmann, I., On the Travel Times of P as Determined From Nuclear Explosions: Bull. Seis. Soc. Amer., vol. 54, pp. 123-139, 1964

12. Mims, C. and Sax, R. L., Rectilinear Motion Detection: paper presented to the Seismological Society of America, April, 1965

13. Press, F. and Archambeau, C. B., Release of Tectonic Strain by Underground Nuclear Explosions: J. Geoph. Res., vol. 67, 1962

14. Romney, C., Brooks, B. G., Mansfield, R. H., Carder, D. S., Jordan, J. N., and Gordon, D. W., Travel Times and Amplitudes of Principle Body Phases Recorded From Gnome: Bull. Seis. Soc. Amer., vol. 52, pp. 1057-1074,

15. Shimshoni, M. and Smith, S. W., Seismic Signal Enhancement with Three-Component Detectors: Geophysics, vol. 24, pp. 664-671, 1964

16. Toksoz, M. N., Harkrider, D. G., and Ben Menahem, A., Determination of Source Parameters by Amplitude Equalization of Seismic Waves: II. Release of Strain by Underground Nuclear Explosions: J. Geoph. Res., vol. 69, pp. 4355-4366, 1964

LIST OF ILLUSTRATIONS

Figures

Figures

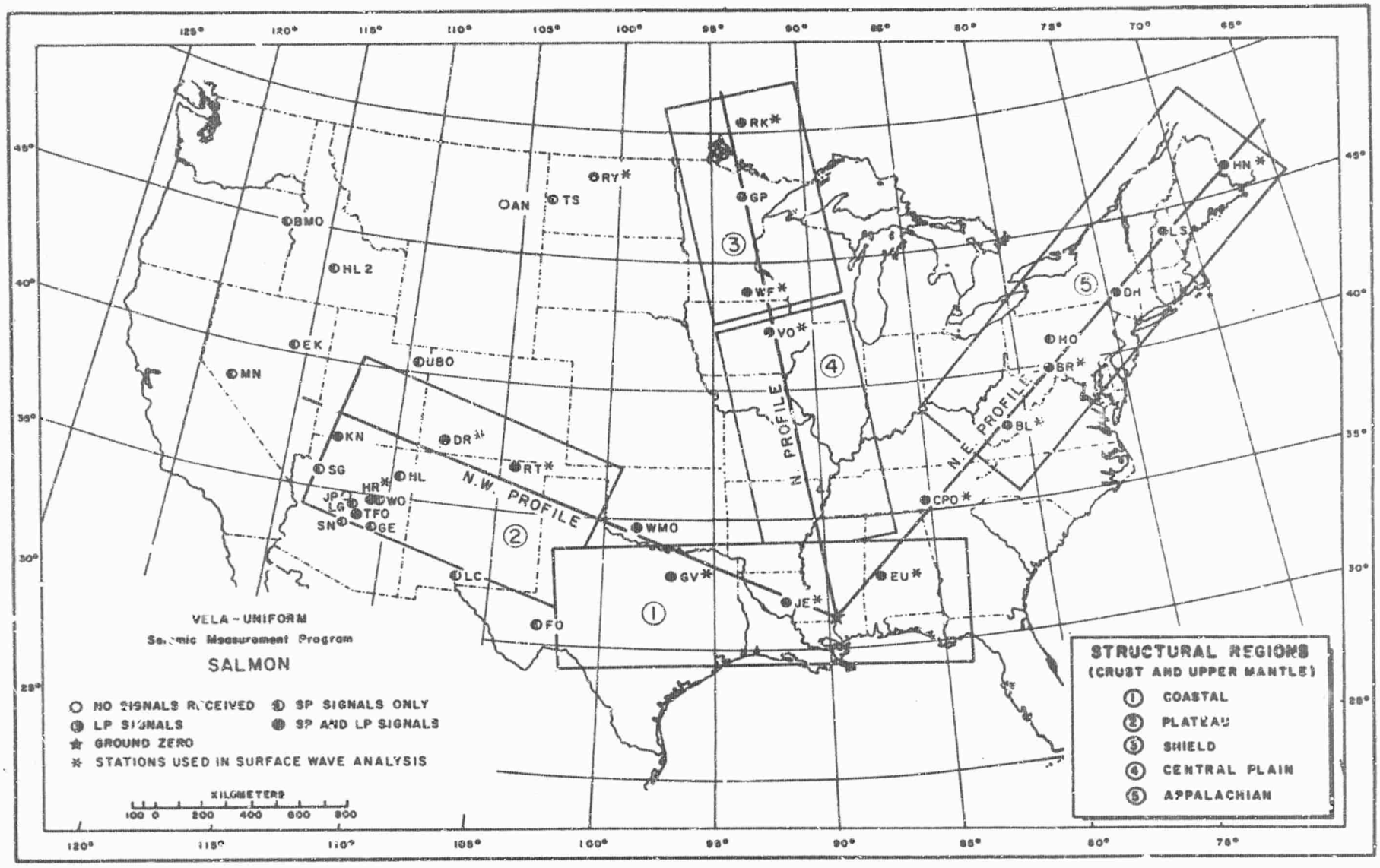

Station Locations, Signal Reception, Structural Regions and Station-Source Profile

Figure 1

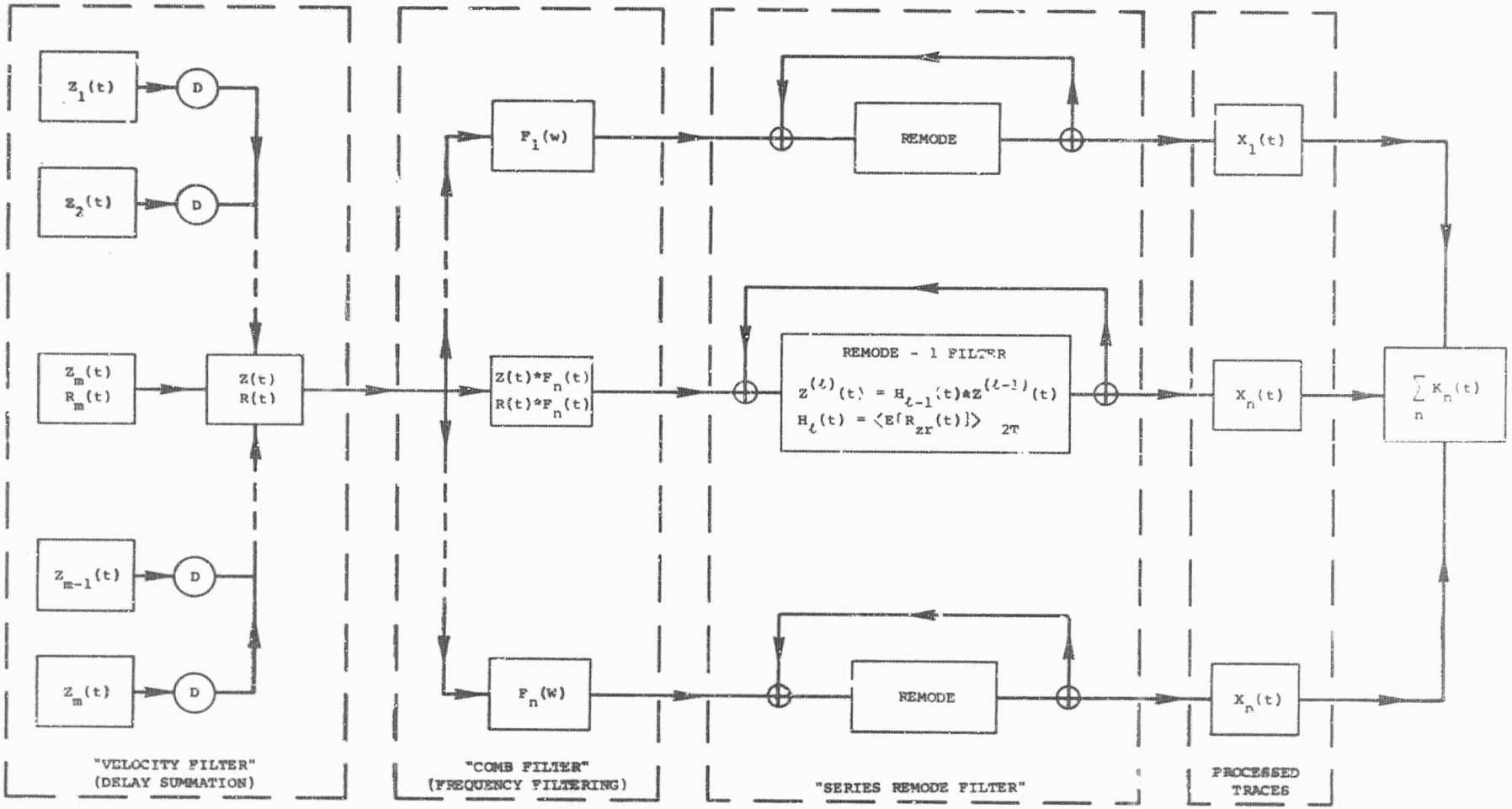

REMODE Array Processor

Figure 2

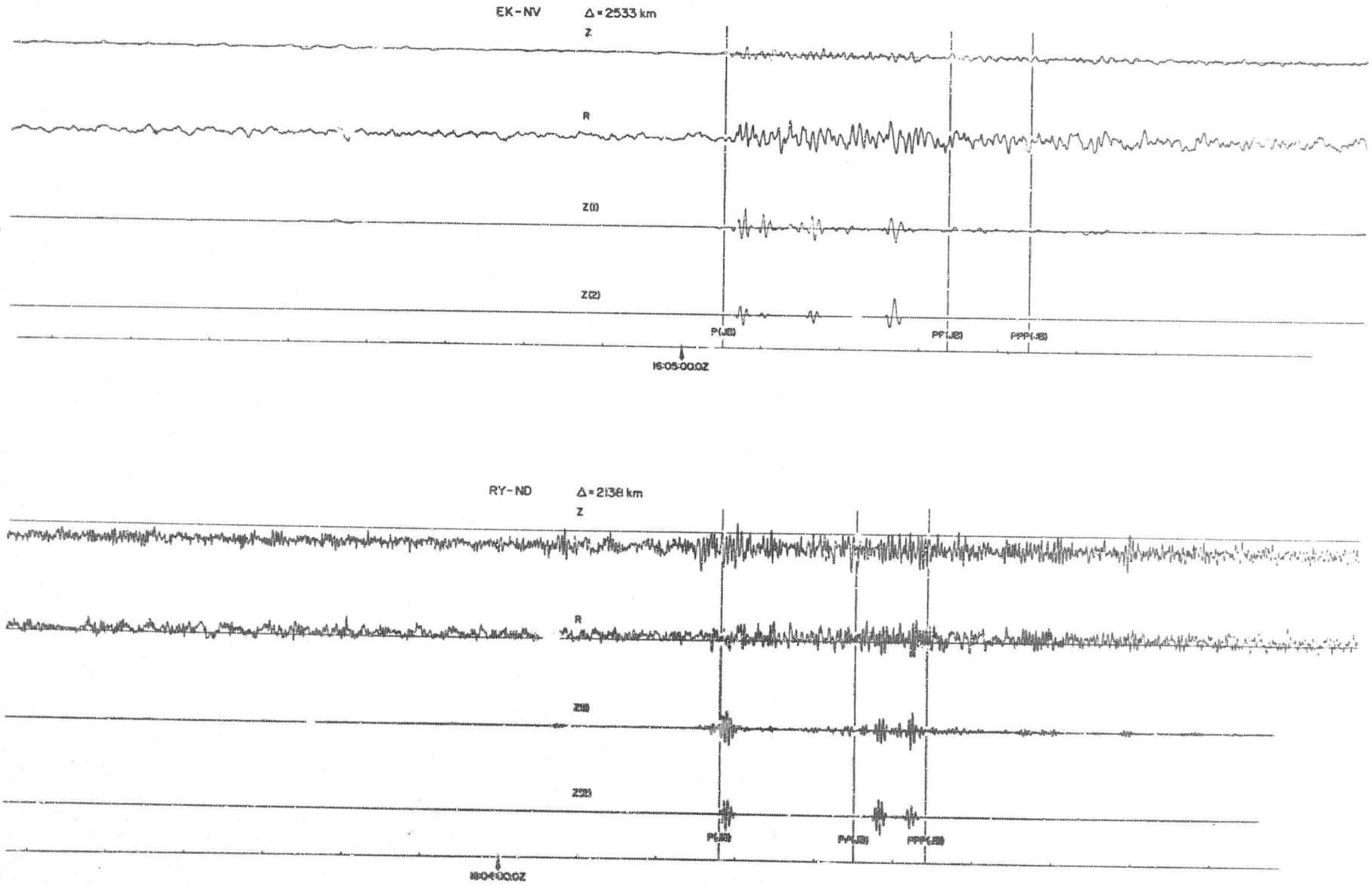

REMODE Seismograms for SALMON (EK-NV and RY-ND)

Figure 3

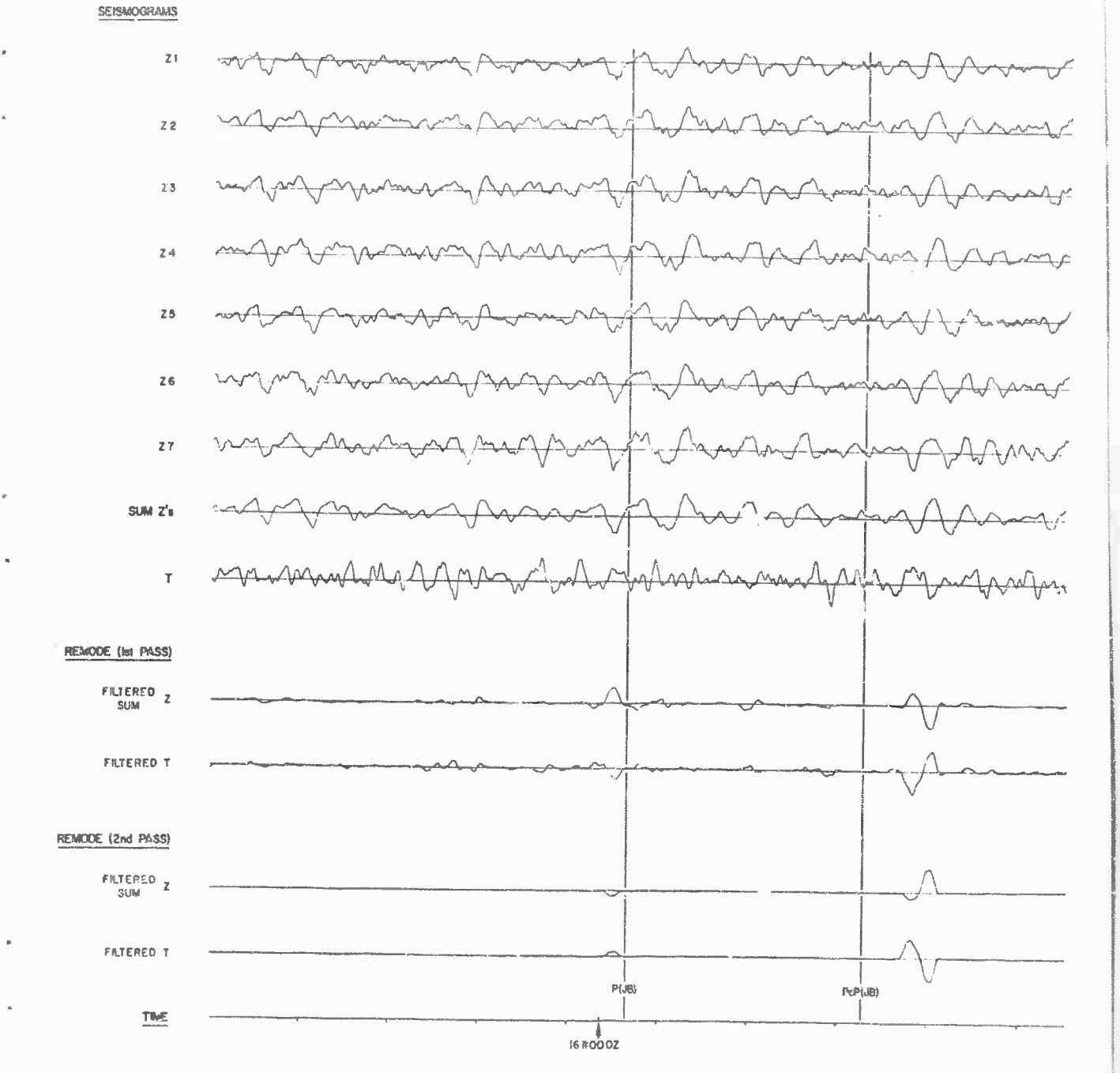

REMODE Array Processed Seismograms for OSLO, NORWAY,

Δ = 7565 Km, SALMON Event

Figure 4

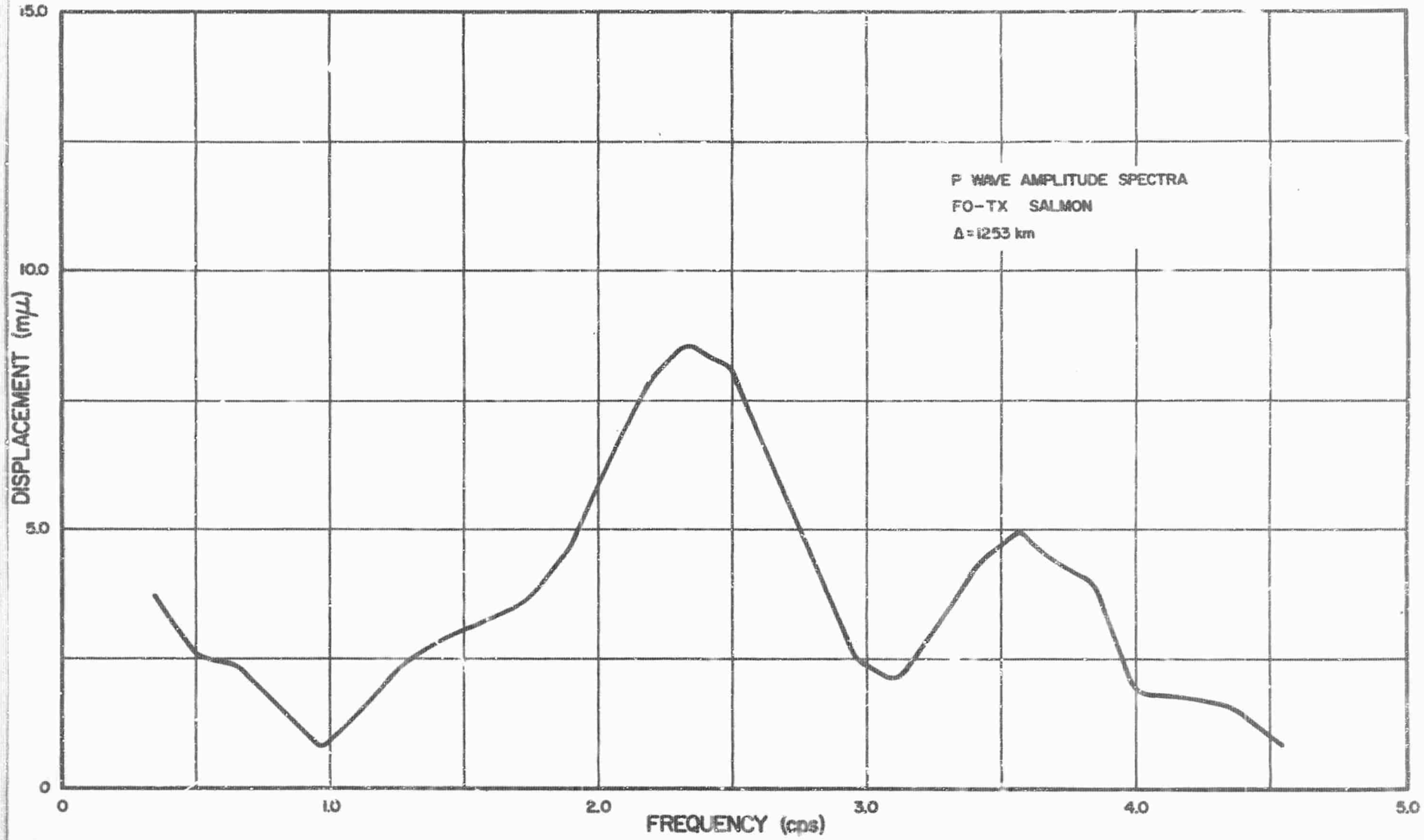

P_n Wave Amplitude Spectra, Station FO-TX, Δ = 1253 Km, SALMON Event

Figure 5

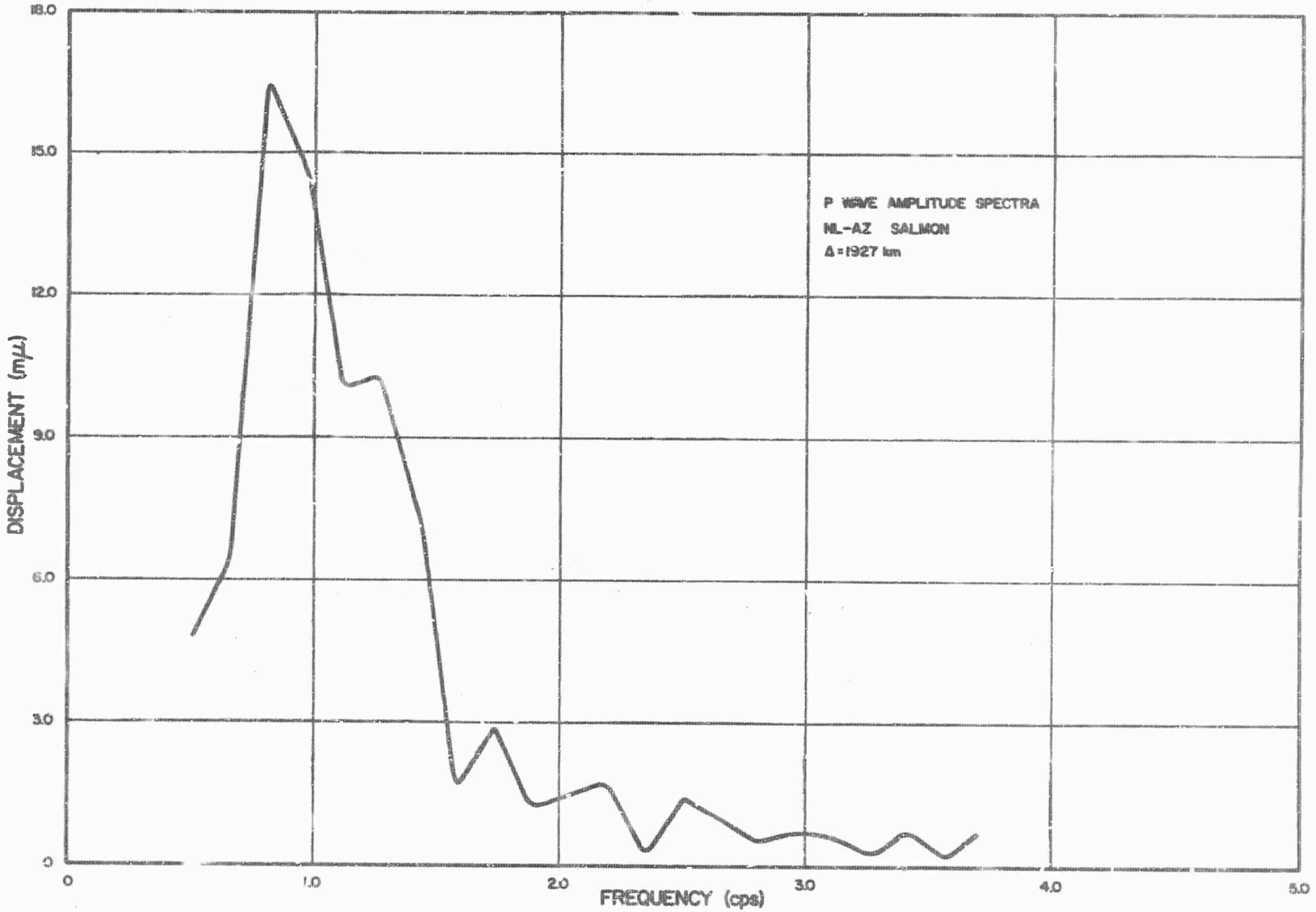

P Wave Amplitude Spectra, Station NL-AZ, Δ = 1927 Km, SALMON Event
(P_2 branch of travel time curve)

Figure 6

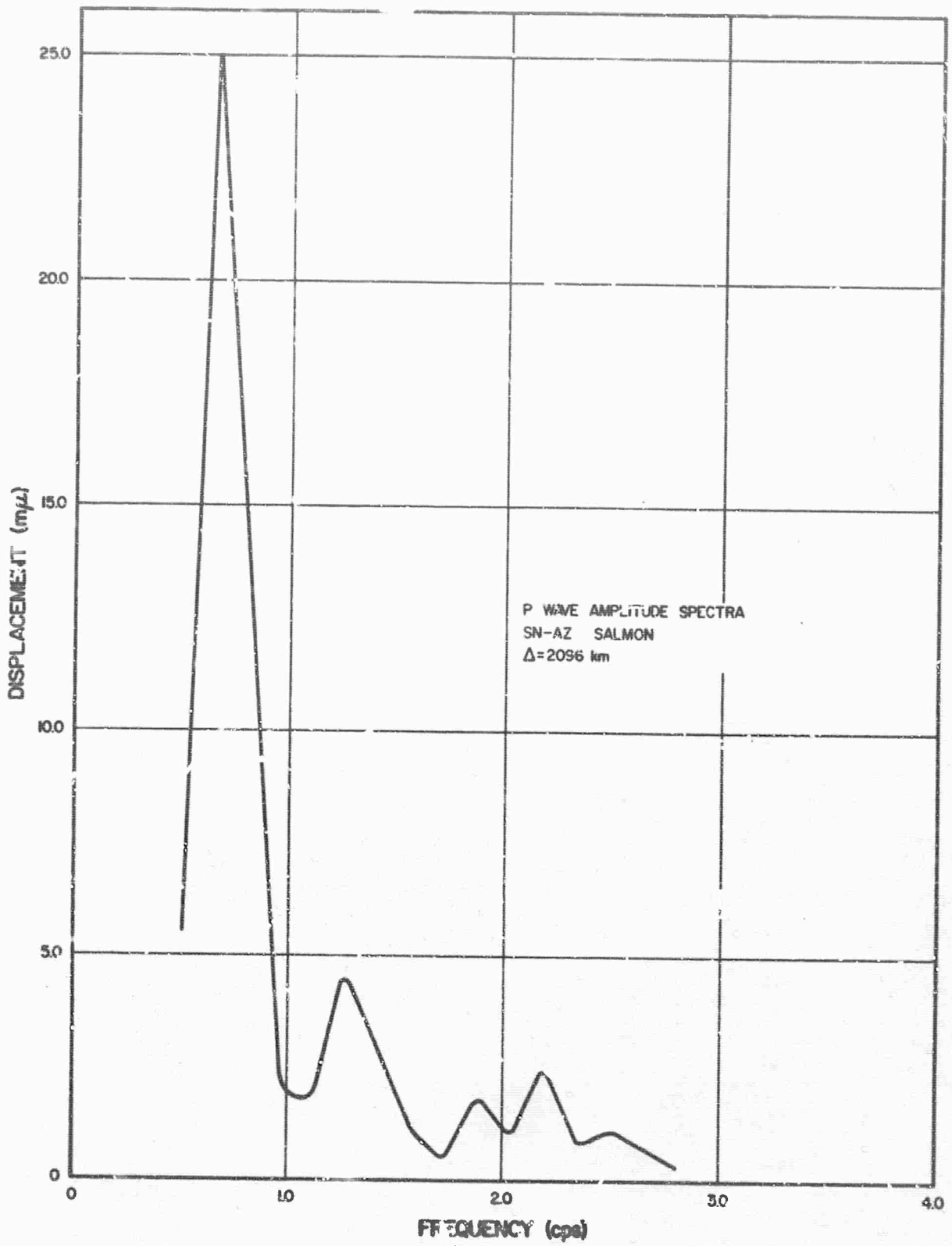

P Wave Amplitude Spectra, Station SALMON Event SN-AZ, Δ = 2096 Km, (P_2 branch of travel time curve)

Figure 7

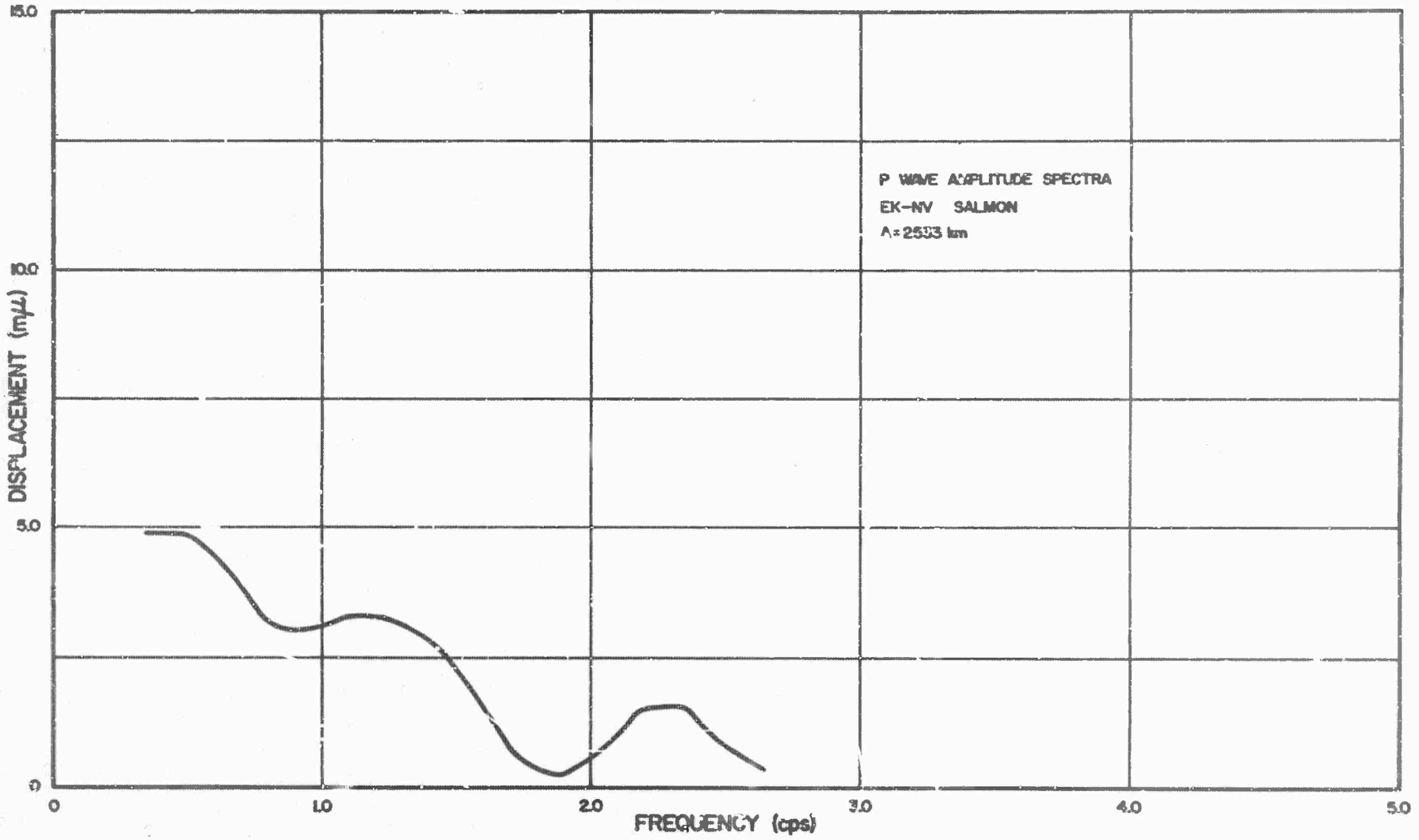

P Wave Amplitude Spectra, Station EK-NV, Δ = 2533 Km, SALMON Event
(P_2 branch of travel time curve)

Figure 8

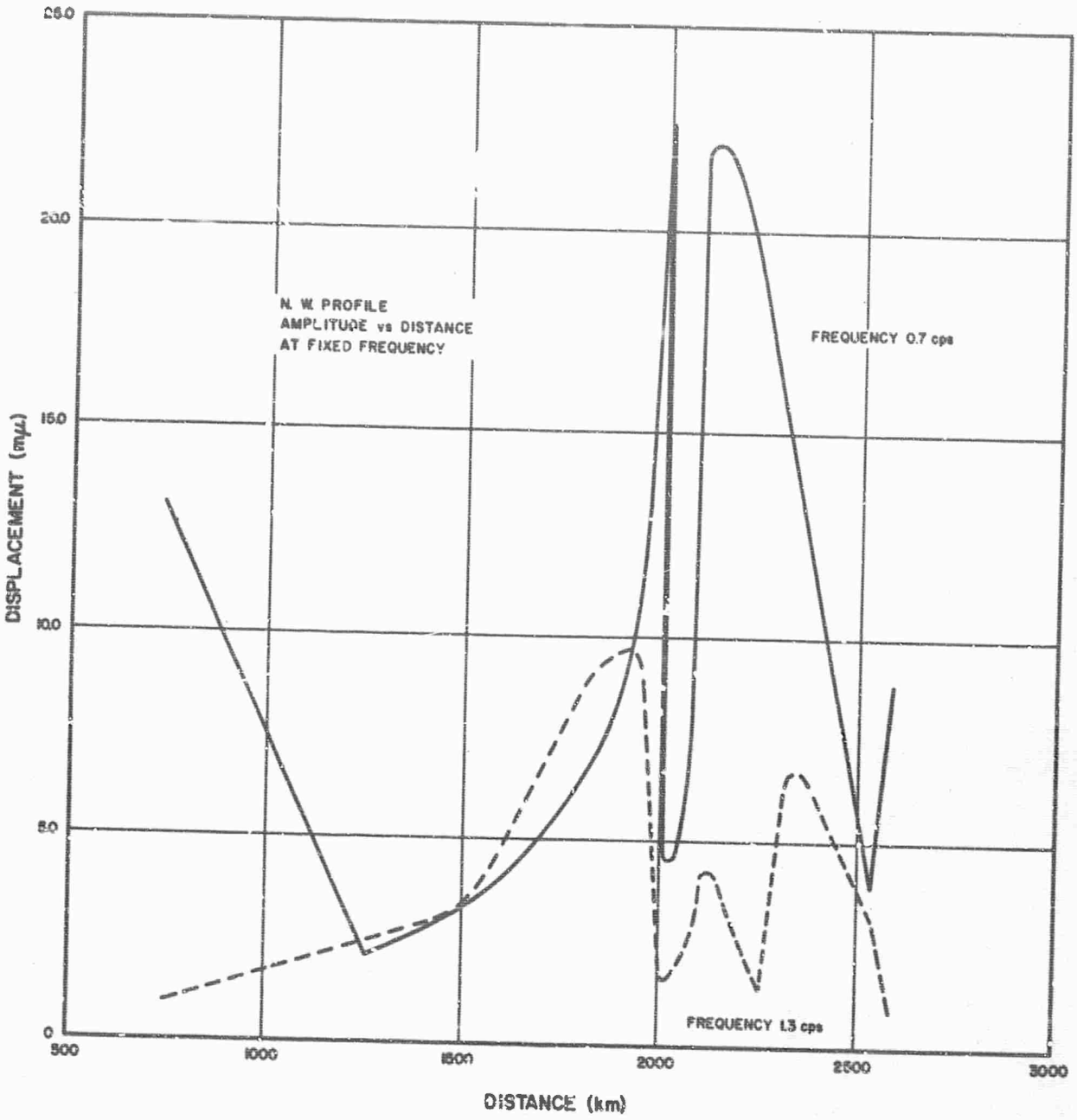

Amplitude versus Distance at Fixed Frequencies, N. W. Profile

Figure 9

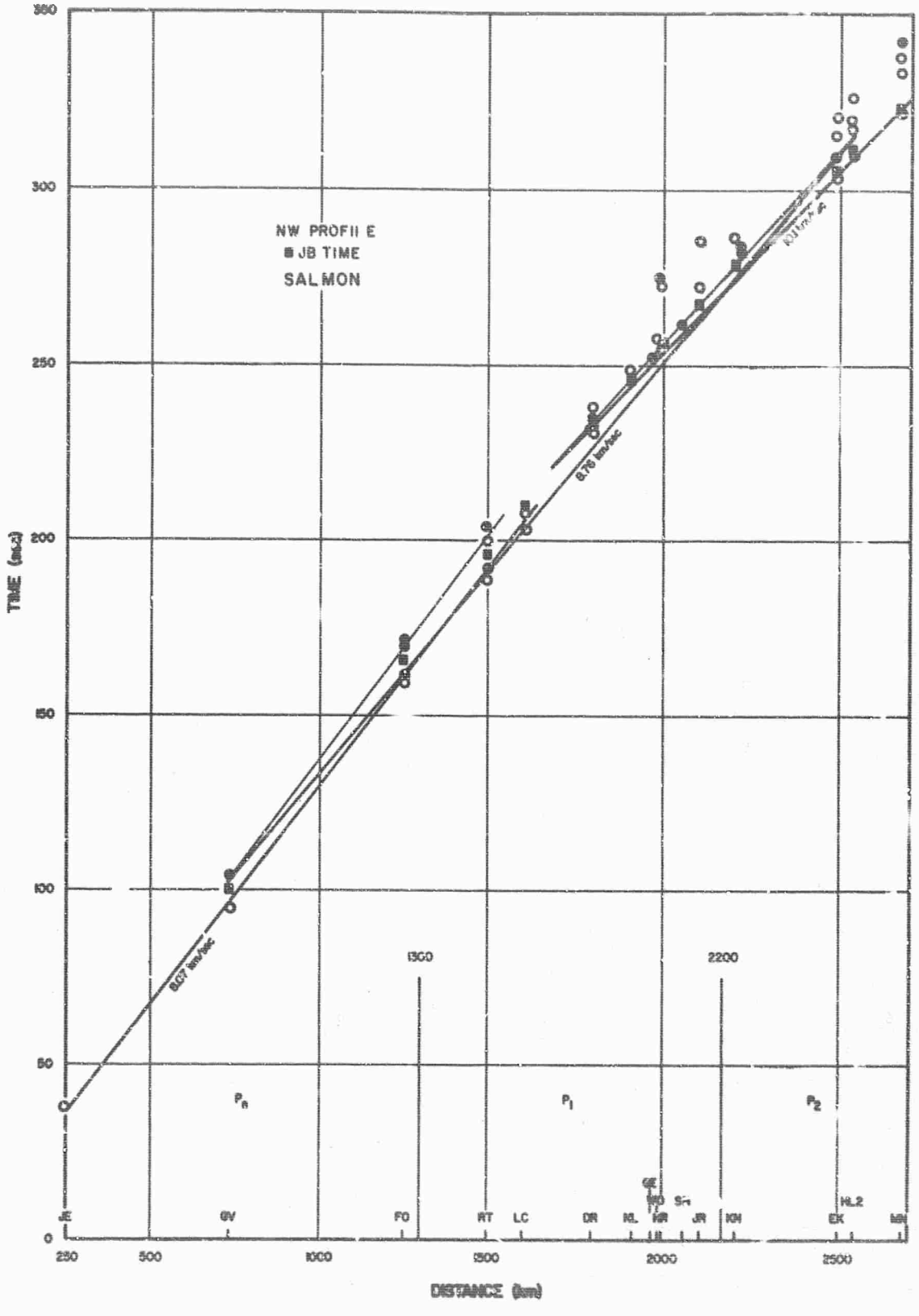

Travel Times versus Distance, N. W. Profile, SALMON Event

Figure 10

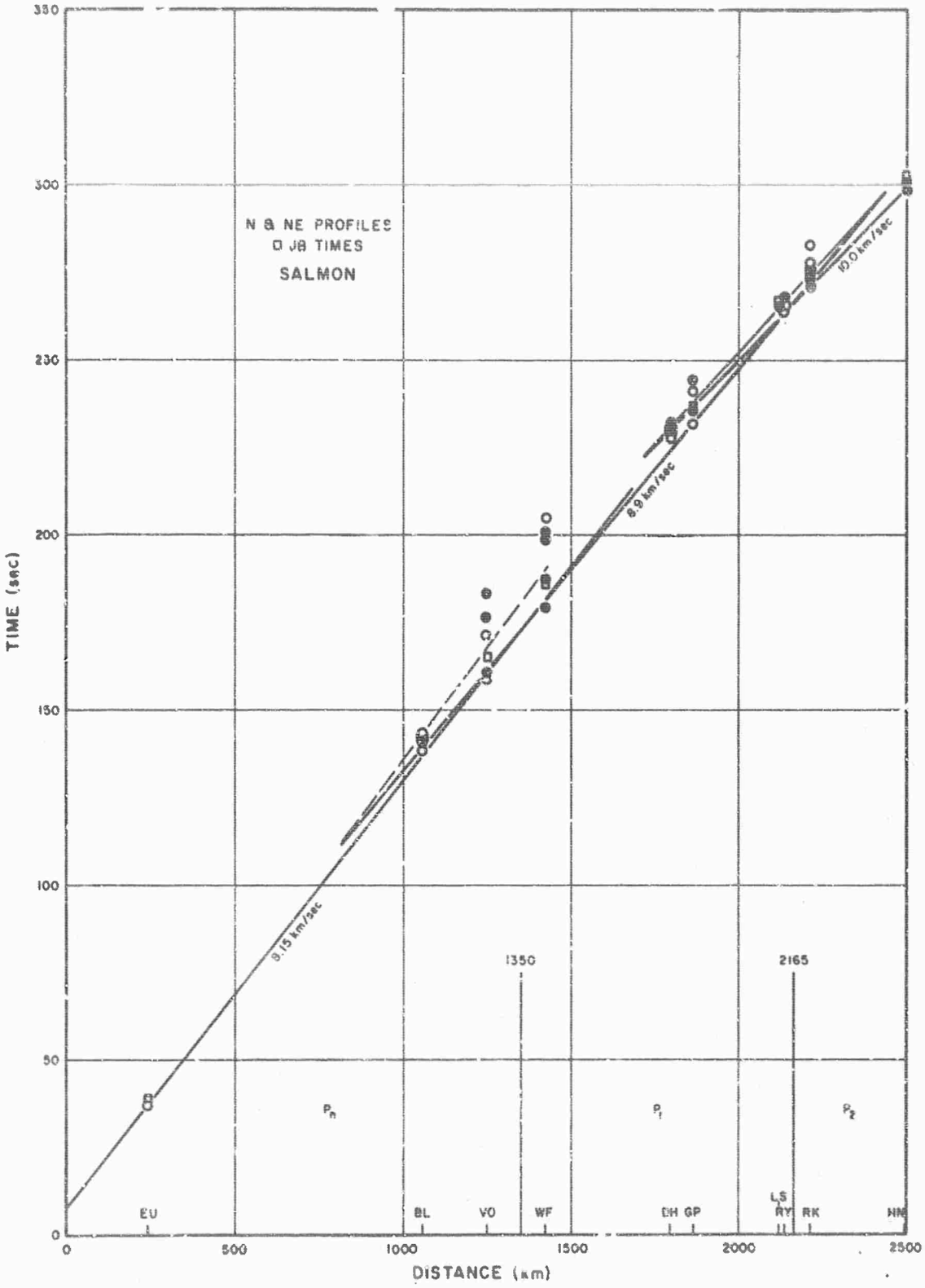

Travel Times versus Distance, Combined N. and N. E. Profiles, SALMON Event

Figure 11

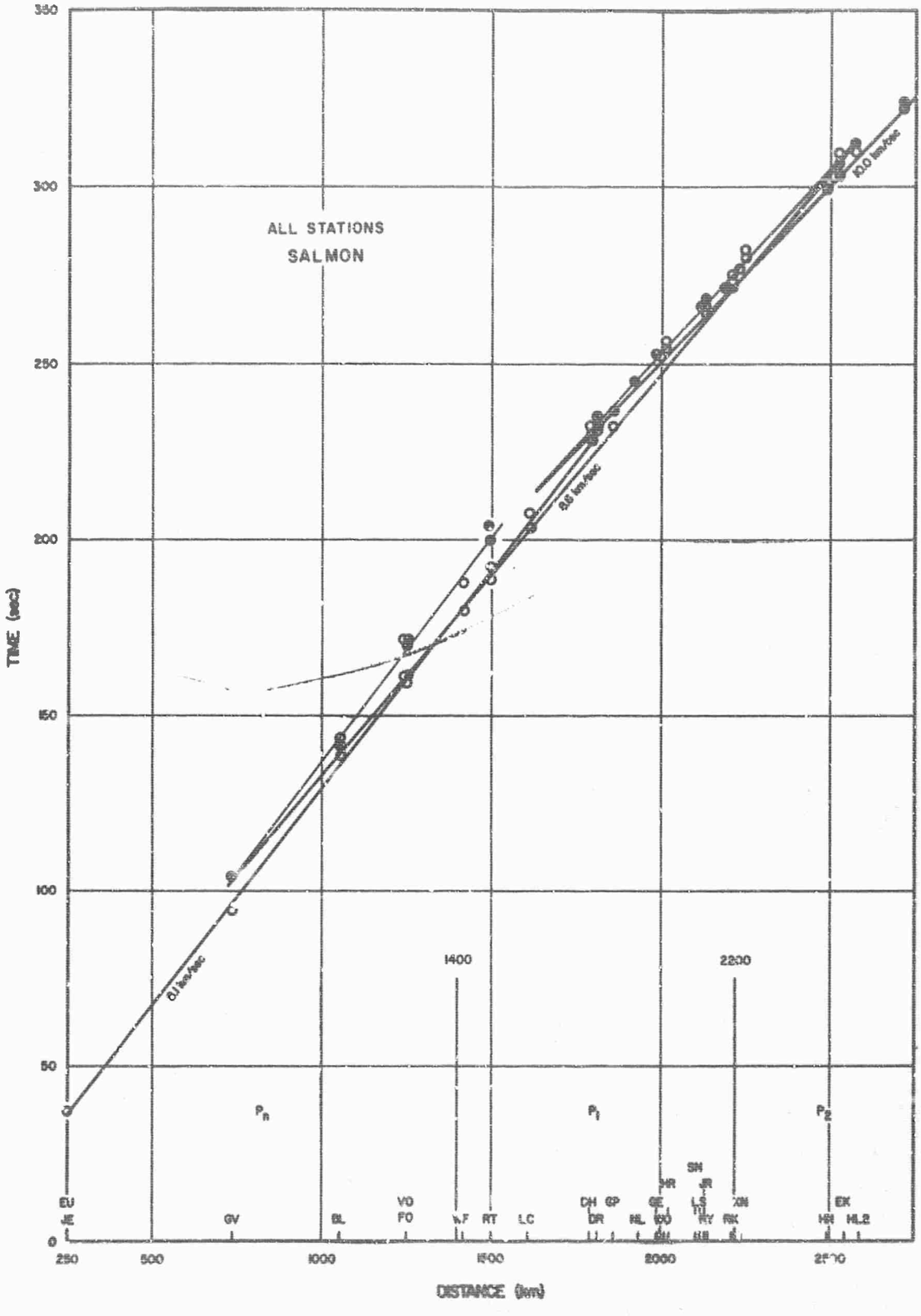

Travel Times versus Distance, All Profiles Combined, SALMON Event

Figure 12

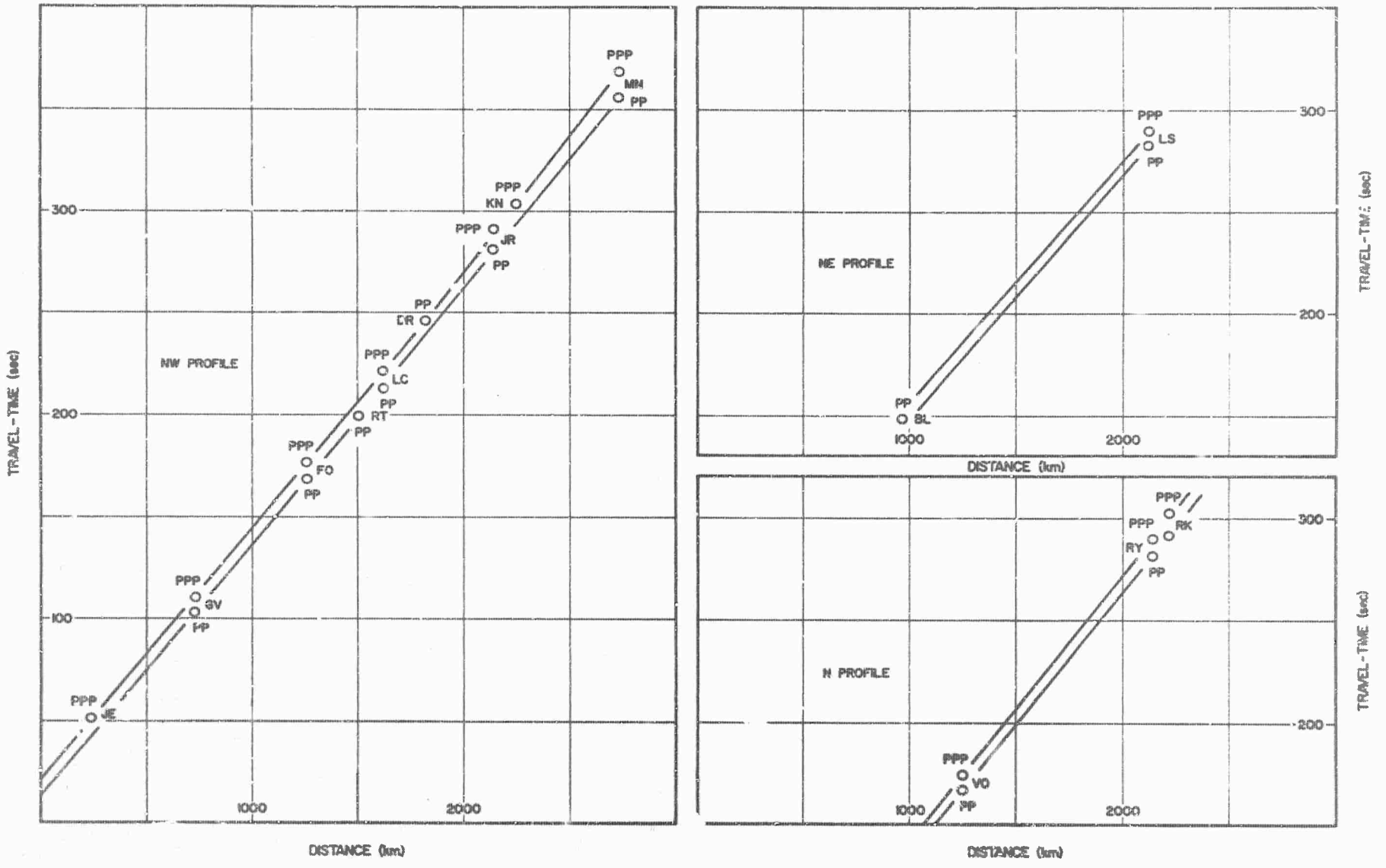

Travel Times for PP and PPP on N, NE, NW Profiles, SALMON Event

Figure 13

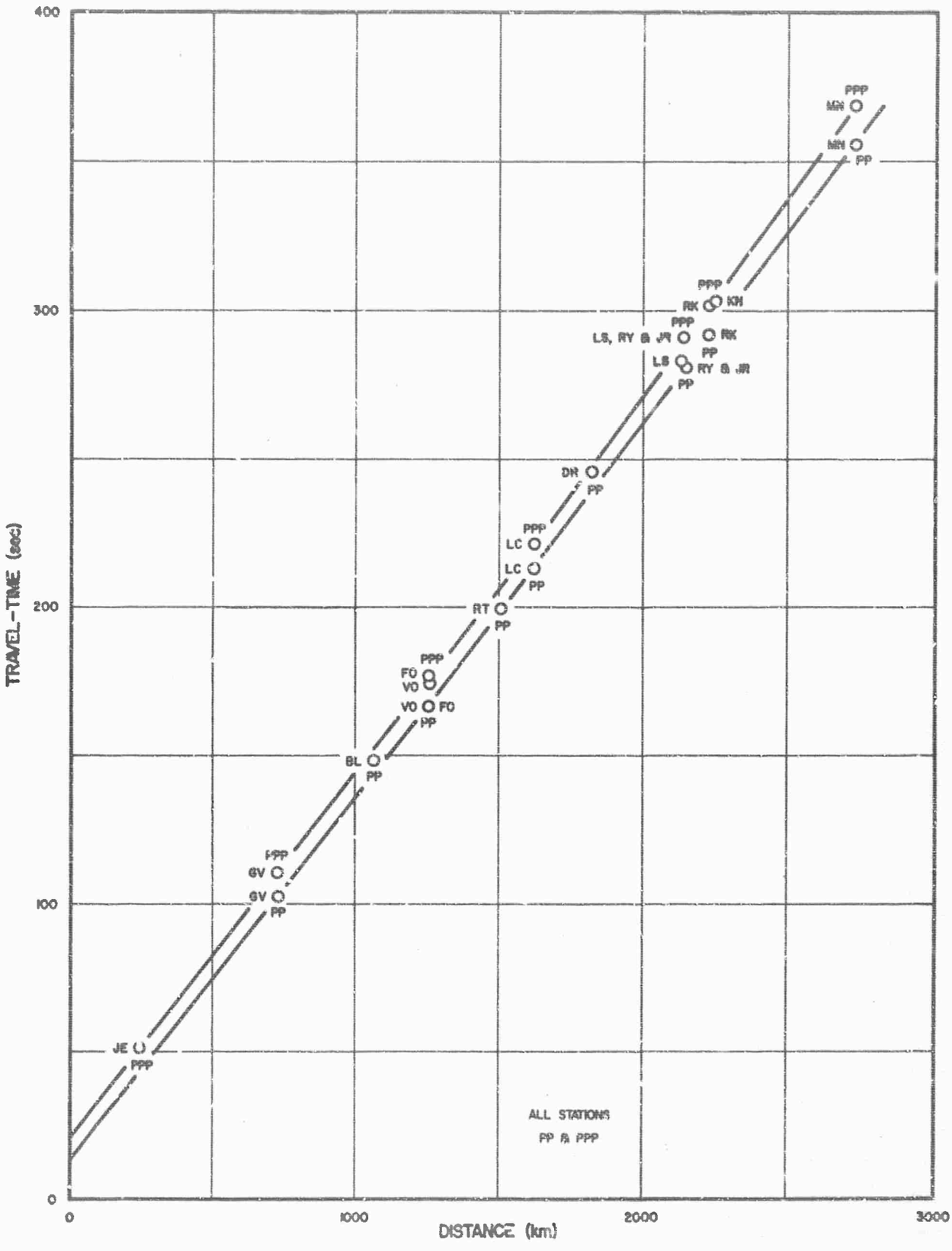

Travel Times for PP and PPP on all Profiles, SALMON Event

Figure 14

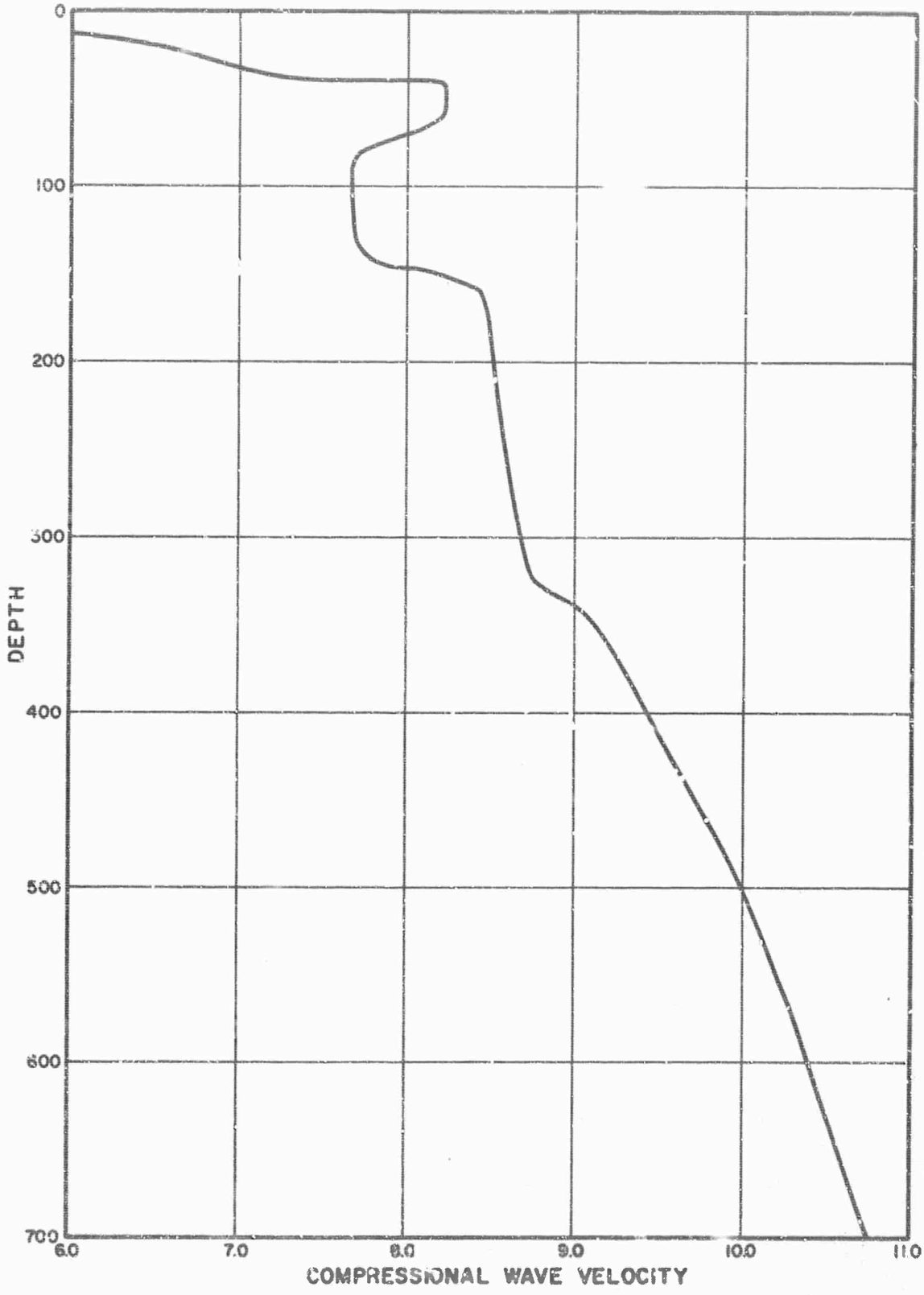

Preliminary Compressional Velocity Structure
to Appropriate Travel Time Observations, SALMON Event

Figure 15

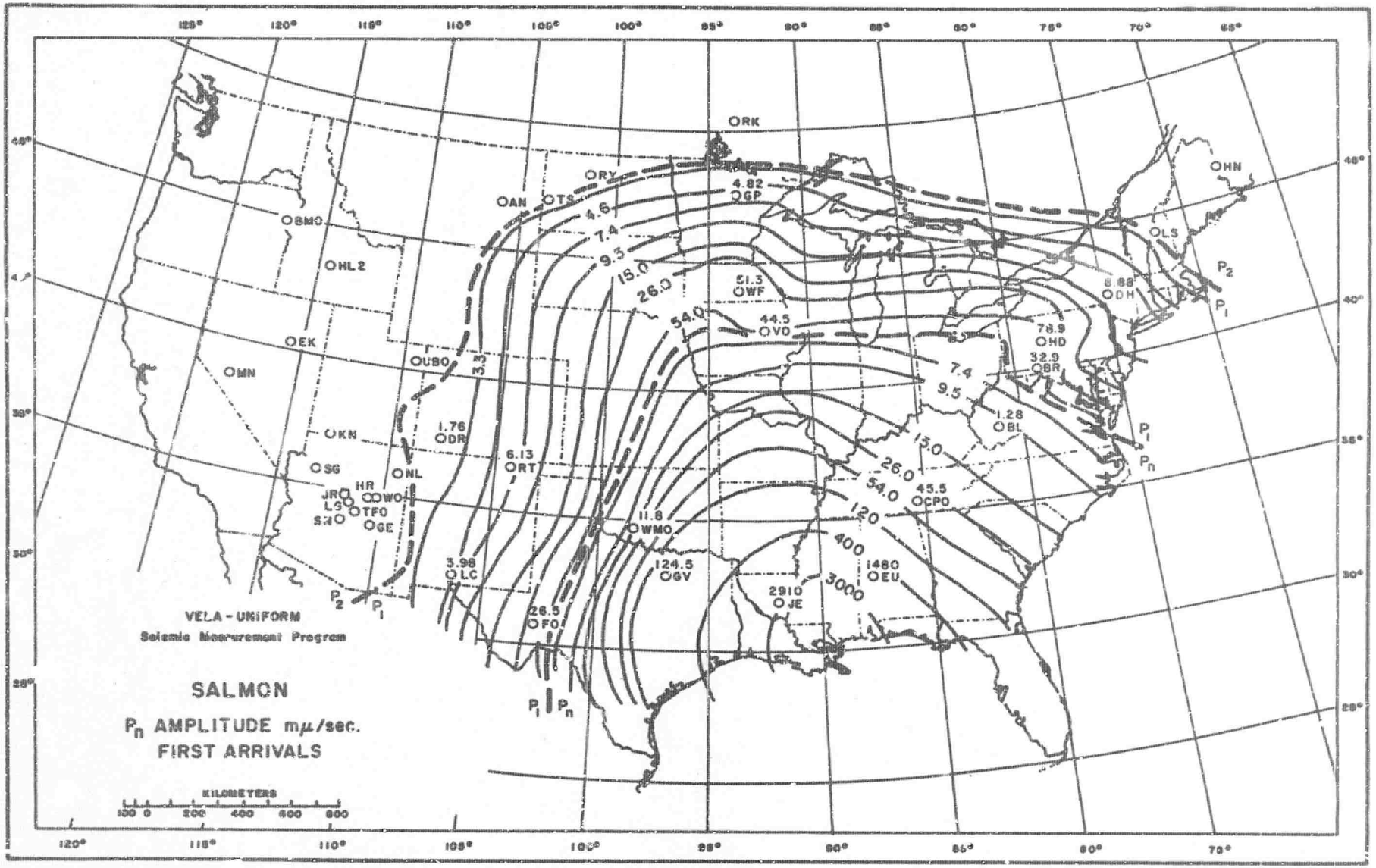

Radiation Patterns for P_n and P Phases

Figure 16

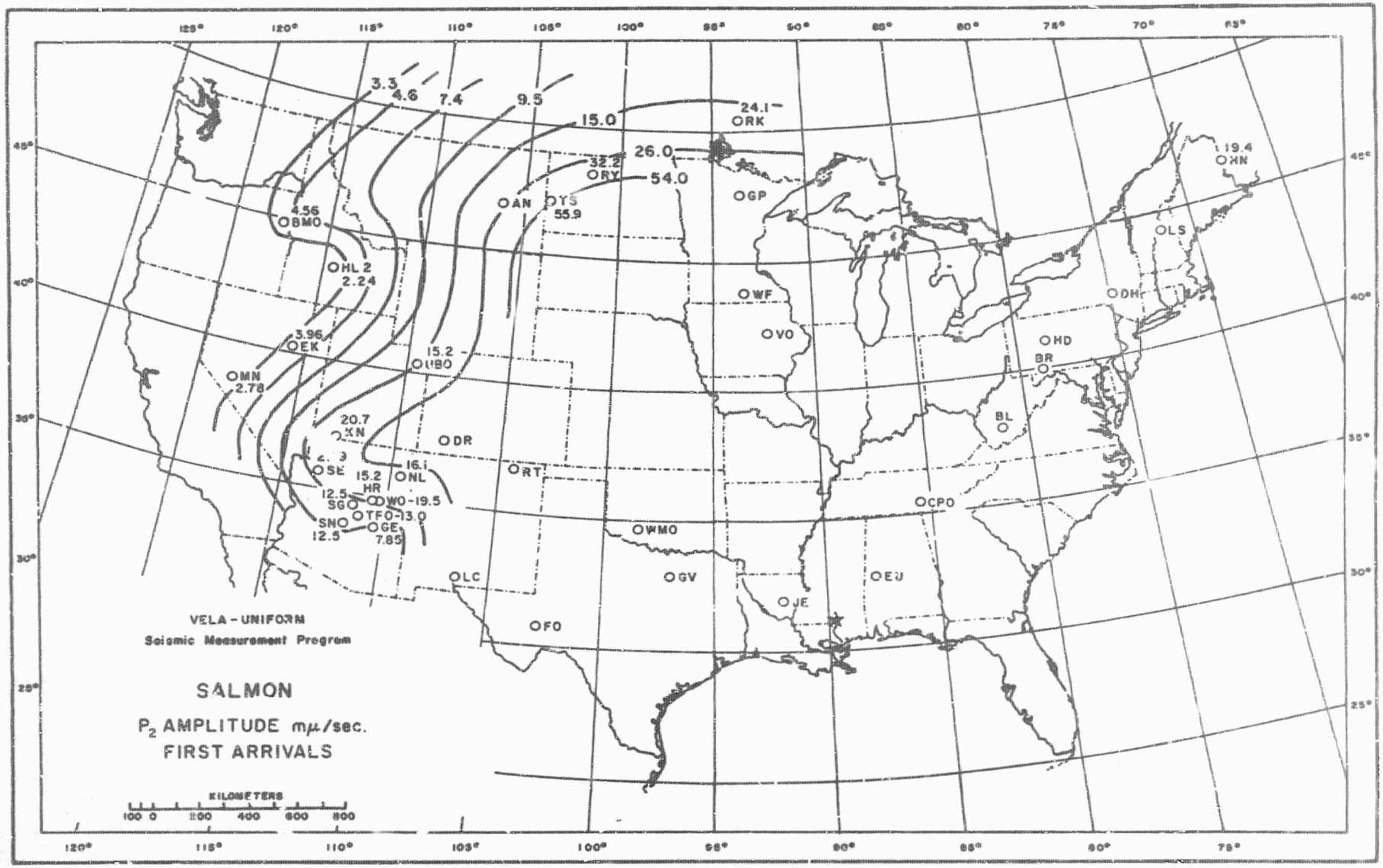

Radiation Patterns for P_2 Phases

Figure 17

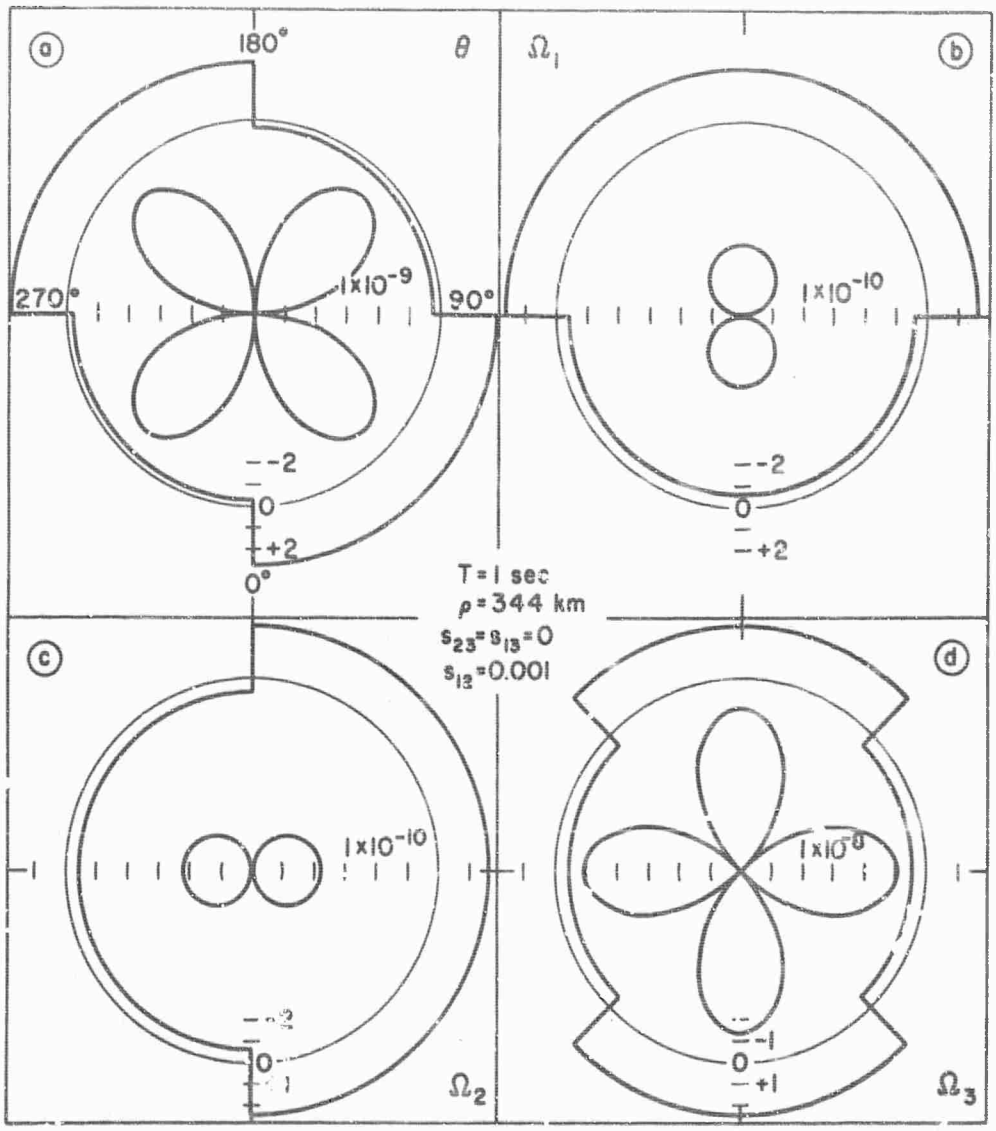

Theoretical Radiation Patterns for P and S Wave Radiation
Due to Shock Induced Tectonic Energy Release

Figure 18

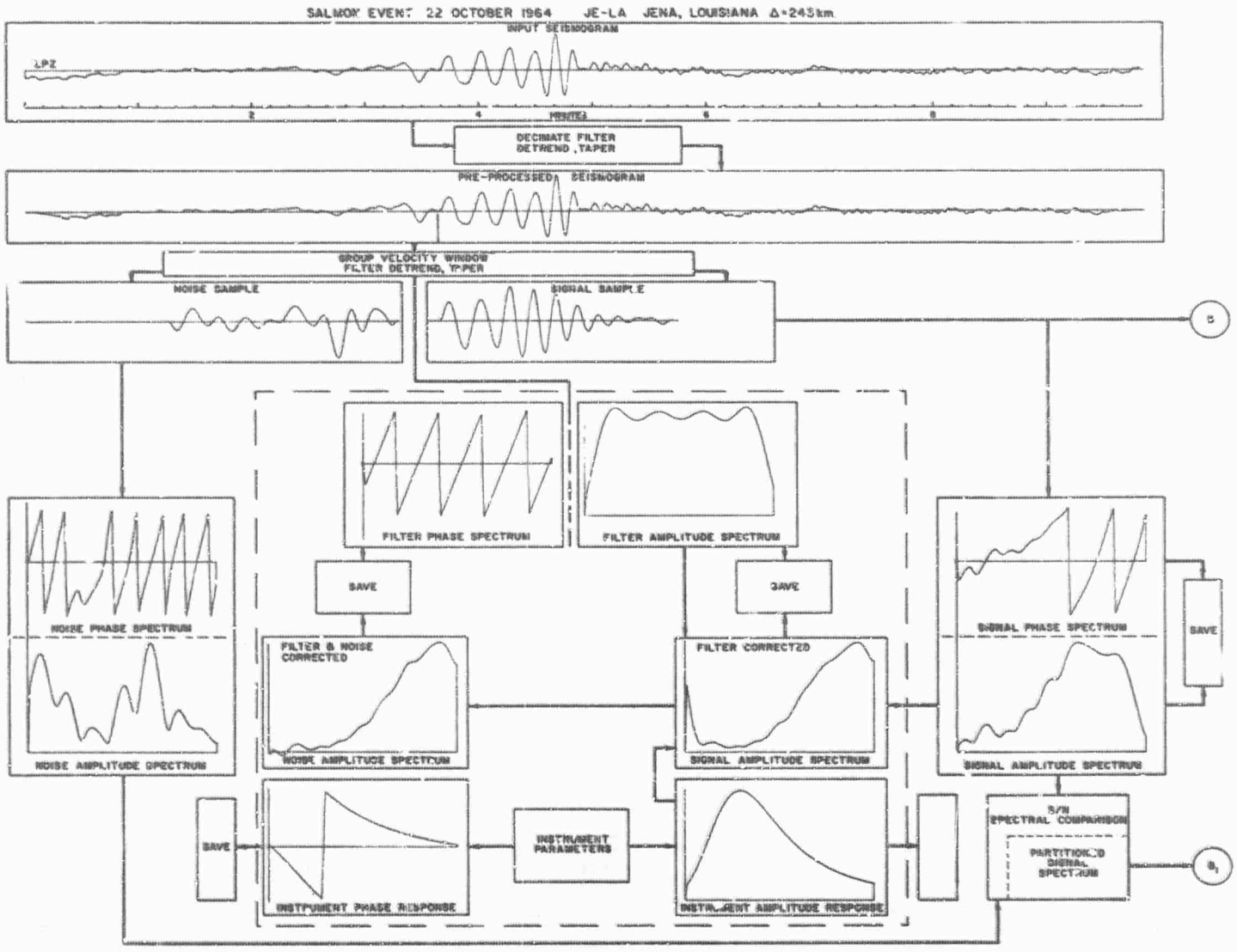

Flow Diagram of Seismic Wave Analysis Program (SW-AP-8)

Section A - Amplitude and Phase Spectra

Figure 19

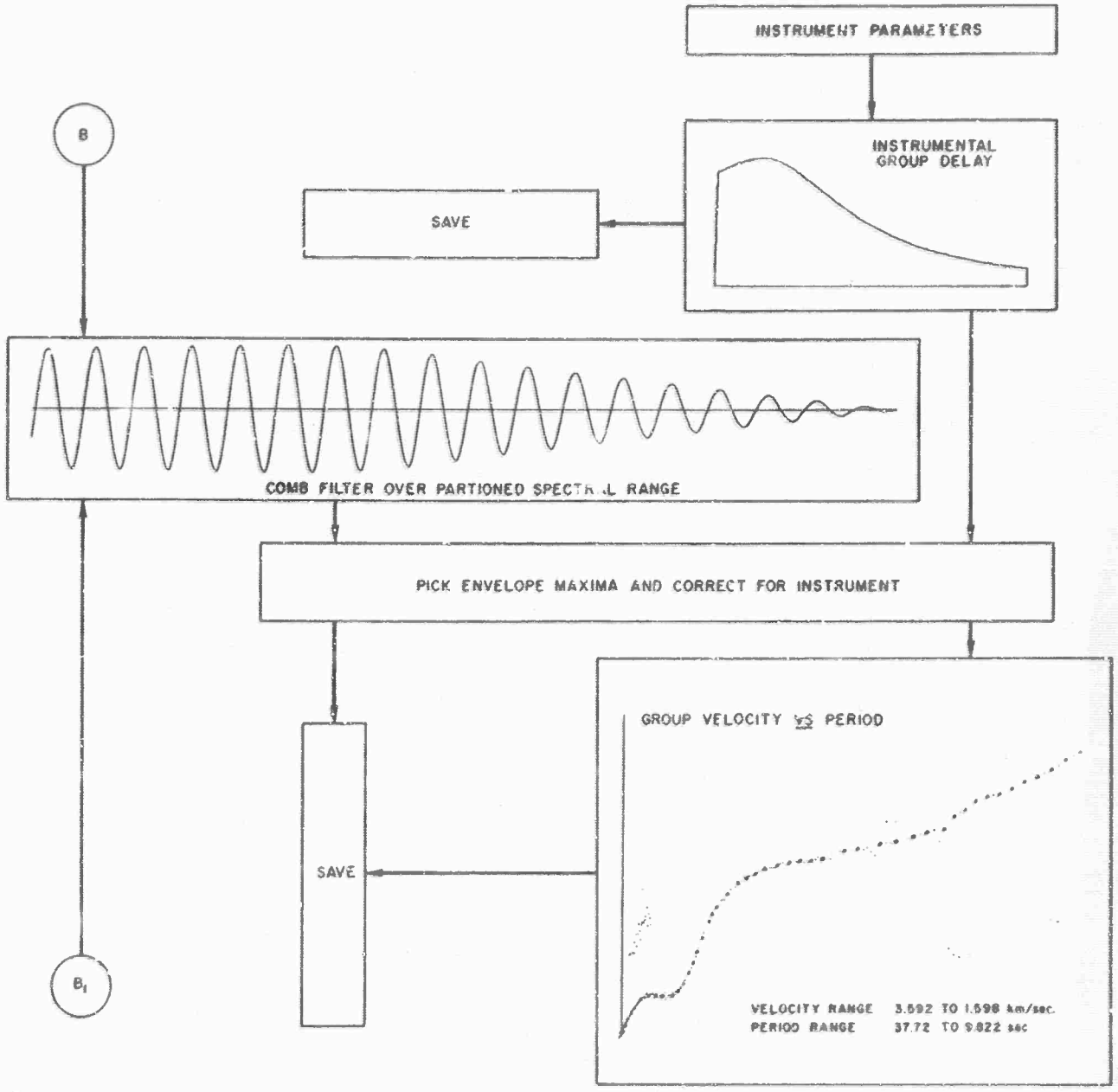

Flow Diagram of Seismic Wave Analysis Program (SW - AP-8)

Section B - Group Velocity Analysis

Figure 20

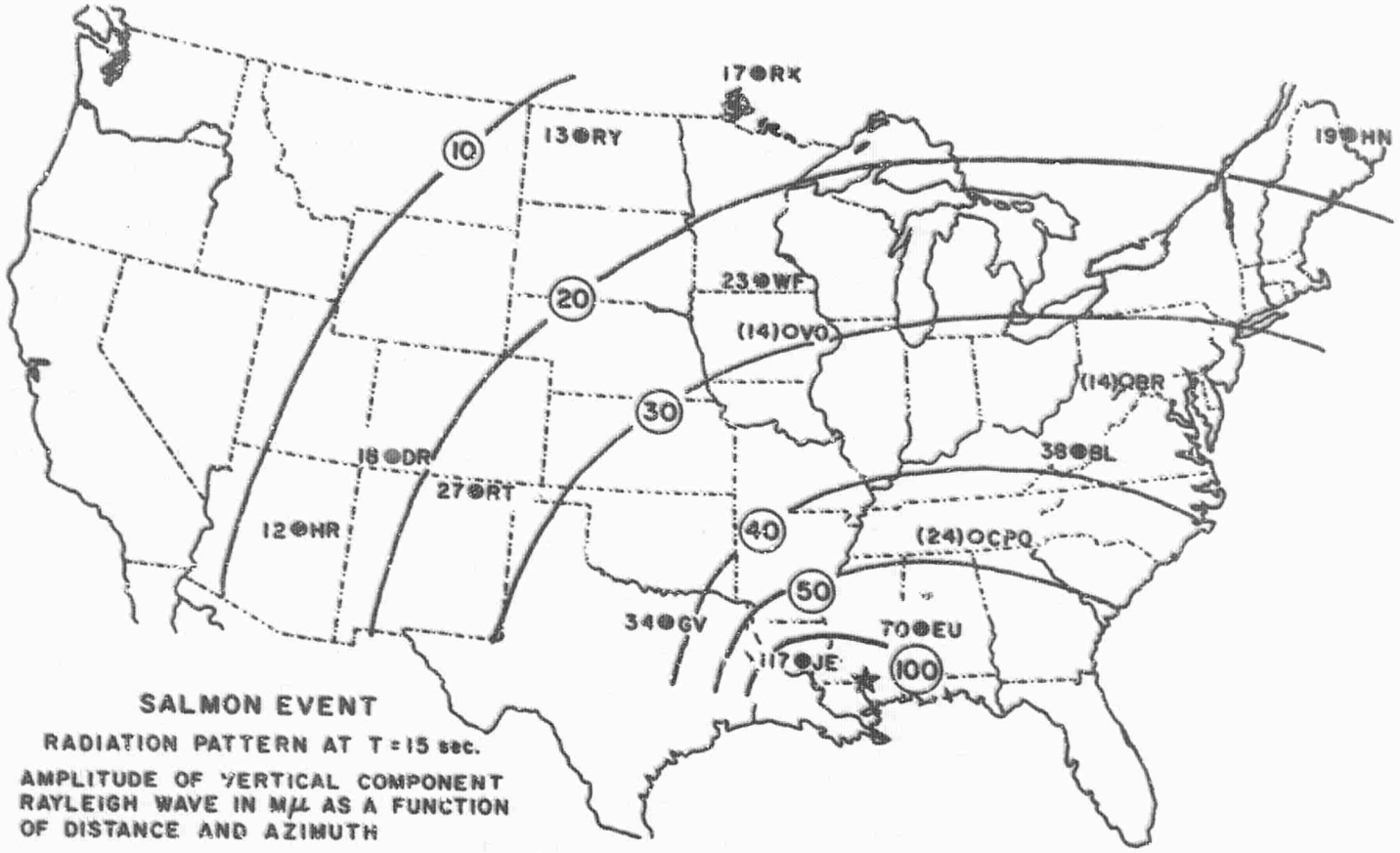

Rayleigh Wave Radiation Pattern at T = 15 sec. Amplitude of Vertical Component Rayleigh Wave in Mμ, as a Function of Distance and Azimuth, SALMON Event

Figure 21